ADVANCED MATERIALS
www.advmat.de

Progress and Perspectives of Thin Film Kesterite Photovoltaic Technology: A Critical Review

*Sergio Giraldo, Zacharie Jehl, Marcel Placidi, Victor Izquierdo-Roca, Alejandro Pérez-Rodríguez, and Edgardo Saucedo**

The latest progress and future perspectives of thin film photovoltaic kesterite technology are reviewed herein. Kesterite is currently the most promising emerging fully inorganic thin film photovoltaic technology based on critical raw-material-free and sustainable solutions. The positioning of kesterites in the frame of the emerging inorganic solar cells is first addressed, and the recent history of this family of materials briefly described. A review of the fast progress achieved earlier this decade is presented, toward the relative slowdown in the recent years partly explained by the large open-circuit voltage (V_{OC}) deficit recurrently observed even in the best solar cell devices in the literature. Then, through a comparison with the close cousin Cu(In,Ga)Se_2 technology, doping and alloying strategies are proposed as critical for enhancing the conversion efficiency of kesterite. In the second section herein, intrinsic and extrinsic doping, as well as alloying strategies are reviewed, presenting the most relevant and recent results, and proposing possible pathways for future implementation. In the last section, a review on technological applications of kesterite is presented, going beyond conventional photovoltaic devices, and demonstrating their suitability as potential candidates in advanced tandem concepts, photocatalysis, thermoelectric, gas sensing, etc.

1. Introduction: Positioning Kesterite in the Thin Film Chalcogenide Photovoltaic Field

Following the recent classification by the European Commission of some elements as critical raw materials (CRM),[1] there is an increasing interest in the development of CRM-free thin film photovoltaic (PV) technologies. Specifically, indium, gallium, and tellurium are classified in this category,[2–5] and urgent actions are deemed necessary for their partial or total substitution in photovoltaic technologies. This requires an upstream design and development of solutions using exclusively CRM-free technologies, together with sustainable processes based on circular economy to ensure the long-term sustainability of these new technologies. In this context, several fully inorganic PV technologies based on earth abundant elements have been investigated in the past years, each of them to more or less extent and with more or less success,[6] aiming to figure out whether it is possible to reach a cost-efficient fully inorganic technological solution using exclusively earth abundant elements. While the answer is not straightforward, some interesting candidates have been proposed in the literature. **Table 1** summarizes these materials by representing more than 30 years of research in CRM-free thin film absorbers.

Considering Table 1, the family of materials generically labeled as "kesterite" due to their structure ($Cu_2ZnSnSe_4$, CZTSe; Cu_2ZnSnS_4, CZTS; and the corresponding solid solution $Cu_2ZnSn(S,Se)_4$, CZTSSe) has achieved so far the highest photovoltaic conversion efficiencies among the emerging CRM-free technologies, with values in the 11–13% range.[15–17] This family of materials is closely related to the more mature $Cu(In,Ga)(S,Se)_2$ (CIGSSe) technology, already at a commercial stage[19] with reported PV performances comparable to multicrystalline silicon. The CZTSSe structure is obtained by substitution of two indium (In^{+3}) or gallium (Ga^{+3}) atoms in the CIGSSe structure with one tin (Sn^{+4}) and one zinc (Zn^{+2}) atoms.[20] Additionally, the CZTSSe system can adopt three different structural phases including kesterite, stannite, or primitive mixed Cu–Au as described elsewhere,[21] and the kesterite one was demonstrated as the most stable structural polytype.

Dr. S. Giraldo, Dr. Z. Jehl, Dr. M. Placidi, Dr. V. Izquierdo-Roca, Prof. A. Pérez-Rodríguez, Dr. E. Saucedo
Catalonia Institute for Energy Research (IREC)
Jardins de les Dones de Negre 1, 08930 Sant Adrià de Besòs
Barcelona, Spain
E-mail: esaucedo@irec.cat
Prof. A. Pérez-Rodríguez
IN2UB
Departament d'Enginyeria Electrònica i Biomèdica
Universitat de Barcelona
Martí i Franquès, 1-11, 08028 Barcelona, Spain
The ORCID identification number(s) for the author(s) of this article can be found under https://doi.org/10.1002/adma.201806692.

DOI: 10.1002/adma.201806692

Thanks to this structural similarity with CIGSSe, kesterite materials exhibit excellent properties as photovoltaic absorber including a suitable range of bandgaps ($E_{g\ Cu2ZnSnSe4}$ = 1.0 eV, $E_{g\ Cu2ZnSnS4}$ = 1.5 eV), very high light absorption coefficient (above 10^5 cm^{-1}) and natural p-type conductivity.[22] Together with these properties, the progress made in the past years established kesterite as the most relevant and promising CRM-free fully inorganic thin film candidate for large scale PV deployment to this date.

Starting with the performance breakthrough reported by IBM in 2010,[23] the efficiency of kesterite-based solar cells steadily progressed in the following years achieving a certified record of 12.6% in 2014,[17] and remaining unbeaten till recently, where a new certified record efficiency exceeding 13% was obtained but is not published yet.[24] To contextualize the progress achieved by kesterite, **Figure 1** shows the time evolution of kesterite solar cells efficiency from year 0 (first reported working device) up to date, in comparison with the CIGSSe technology. Considering this evolution, we can state that kesterite technology can be seen as in its "twenties," while the more mature CIGSSe already entered its "forties." Though Figure 1 shows CIGSSe at slightly higher efficiencies for a comparable "age" than kesterite, it is also noteworthy that kesterite cells exhibit a slightly higher slope of efficiency increase; in that sense, it is expected that kesterite could reach a similar level of maturity (efficiencies approaching or overpassing 20%) within the next decade.

To accelerate this technological maturation, it is necessary to first consider which kind of strategies allowed the CIGSSe material to reach its current efficiency level. **Figure 2** presents a direct comparison of some of the best efficiencies (Figure 2a) and lowest open-circuit voltage deficits (V_{OC} deficit, Figure 2b) reported for kesterite and chalcopyrite as a function of the bandgap of the absorber.

The V_{OC} deficits are calculated in this article with respect to the maximum theoretic value represented by the Shockley–Queisser limit.[27] In that regard, the different bandgaps of the materials are considered, hence making the comparison realistic. Then, the V_{OC} deficit is estimated as (Equation (1))

$$V_{OC}\ \text{deficit}\,(\text{mV}) = V_{OC(\text{Shockley–Queisser})}\,(\text{mV}) - V_{OC(\text{measured})}\,(\text{mV}) \quad (1)$$

where the $V_{OC(Shockley–Queisser)}$ is the maximum thermodynamic V_{OC} achievable for a given absorber bandgap, and the $V_{OC(experimental)}$ is the V_{OC} obtained from the J–V analysis under AM1.5G conditions. Most commonly, the bandgap value used for estimating the $V_{OC(Shockley–Queisser)}$ is extracted from the external quantum efficiency (EQE) or internal quantum efficiency (IQE) (a detailed description and comparison of the methods for extracting the bandgap has been published recently by Carron et al.[28]).

Interestingly, both technologies yield very close efficiencies in the case of narrow and wide bandgap absorbers, with an absolute difference of only 1–3% (see Figure 2a for comparing $CuInSe_2$ with $Cu_2ZnSnSe_4$ and $CuInS_2$ with Cu_2ZnSnS_4). In the intermediate bandgap region however, this difference is dramatically increased, with CIGSSe outperforming kesterite by almost 10% for E_g = 1.2 eV. This difference is explained in large part by the voltage deficit as presented in Figure 2b. Notably, the V_{OC} deficit for bandgaps close to 1.0 or 1.5 eV are comparable, and one can consider that kesterite is reasonably close to the state of the art of chalcopyrite materials in that range. But, while for kesterite the V_{OC} deficit increases almost monotonically with the bandgap, it is markedly reduced for intermediate

Sergio Giraldo obtained his Ph.D. in 2018 at the Catalonia Institute for Energy Research (IREC). After obtaining the master's degree, he focused his career on sustainable thin film photovoltaic technologies. He was awarded an FPI fellowship from the Spanish Ministry to develop the Ph.D. thesis entitled "Advanced Strategies for High Efficiency Kesterite Thin Film Solar Cells." Over the past years, he has been working to improve the kesterite device performance through innovative doping and optimization strategies.

Zacharie Jehl has a background in solid state physics and obtained his Ph.D. working on ultrathin CIGSe solar cells at the Institute for Research and Development in Photovoltaic Energy (France). He later became an assistant professor in Japan (Aoyama Gakuin University), working on various thin film solar cells for tandem application, before joining the University of Tokyo to focus his research on 3rd generation photovoltaics (Hot Carriers). Awarded with a TECNIOspring/Marie Curie Scholarship in 2018, he joined the Catalonia Institute for Energy Research and focuses his work on innovative wide-bandgap absorbers and numerical modeling of Kesterite solar cells.

Edgardo Saucedo is the Deputy Head of the Solar Energy Materials and Systems Laboratory at the Catalonia Institute for Energy Research (IREC) in Barcelona, Spain. He has supervised ten Ph.D. theses in the photovoltaic field. He is currently the coordinator of the research and innovation H2020 project STARCELL (www.starcell.eu), and the RISE (Marie Curie) project INFINITE-CELL (www.infinite-cell.eu).

Table 1. Summary of selected relevant CRM-free fully inorganic PV technologies reported up to date, including the record conversion efficiencies so far (listed from the simplest to the most complex from a structural point of view). Organic or hybrid organic/inorganic PV technologies like perovskites are out of the scope of this review.

Material	Eff.[%]	V_{OC}[mV]	J_{SC}[mA cm^{-2}]	FF[%]	Main technological challenge	Ref.
Se	6.5	969	10.6	63.4	Optimization of buffer layer and increasing lifetime.	[7]
Cu_xS	10.2	599	18.5	74.8	Control of the different phases, and instability due to Cu diffusion.	[8]
Cu_xO	8.1	1100	11.5	60	Control of the different phases and low J_{SC}. High process temperature.	[9]
SnS	4.4	372	20.2	58	Control of the different phases, difficult n-type partner.	[10]
FeS_2	2.8	187	42	50	Phase purity, S content control.	[11]
Zn_3P_2	5.96	492	14.93	71	Low V_{OC} (difficulty to find adequate buffer partner), uncontrolled diffusion of Mg used to dope p-type.	[12]
Cu_3BiS_3	0.09	97	2.9	31.3	High doping level, poor charge transport properties.	[13]
Cu_2SnS_3	4.3	258	35.6	46.7	Doping control, phase purity.	[14]
$Cu_2ZnSnSe_4$	11.8	463	38.3	66.3	V_{OC} deficit.	[15]
Cu_2ZnSnS_4	11.0	731	21.7	69.3	V_{OC} deficit.	[16]
$Cu_2ZnSn(S,Se)_4$	12.6	513	35.2	69.8	V_{OC} deficit.	[17]
$Cu_2BaSn(S,Se)_4$	5.2	611	17.4	48.9	Buffer layer. Carrier density, microstructure, interface engineering.	[18]

bandgaps in the case of chalcopyrite, highlighting the V_{oc} deficit problem largely discussed among the kesterite community. The origin of this issue is still a matter of intensive research and debates; the leading explanations mention deep defects, composition, and bandgap fluctuations introduced by cationic disorder, low carrier's lifetime, secondary phases, etc.[22,33,34]

In the search for technological solutions, one can gather important insights from the evolution of CIGSSe efficiency with time (Figure 1), noting that the most relevant improvements in this technology are commonly related to three important breakthroughs: 1) the incorporation of Na,[35] 2) the introduction of Ga in the alloy,[36] and 3) the postdeposition treatment with K[37] and more recently with Rb and Cs.[38]

In the case of Na, the origin of its beneficial effect on CIGSSe of this doping has been largely discussed in the past 20 years.[39–41]

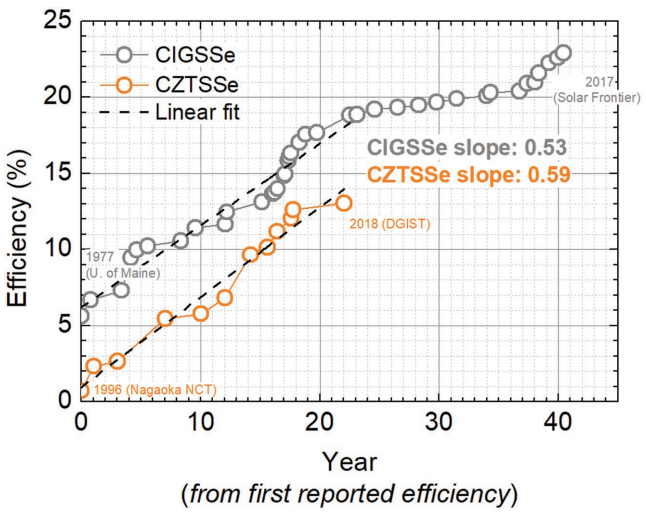

Figure 1. Efficiency evolution of kesterite and chalcopyrite from the first reported working solar cell. Year 0 is 1977 for CIGSSe[25] and 1997 for kesterite.[26]

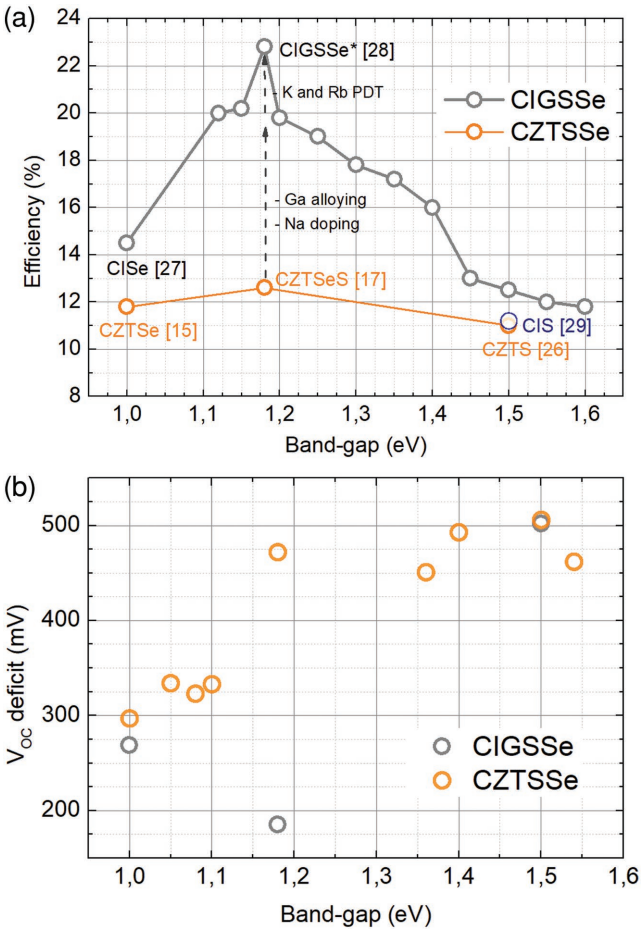

Figure 2. a) Kesterite and chalcopyrite solar cell devices efficiency as a function of the bandgap.[29–31] The values without reference were extracted from Contreras et al.[32] b) Summary of voltage deficits (with respect to the Shockley–Queisser limit)[27] for kesterite and chalcopyrite with values extracted from references of (a).

Grain growth and texturization, interfaces and grain boundaries passivation, impact on In and Ga re-distribution, and control of the carrier concentrations are frequently ascribed to Na incorporation in CIGSSe.[35,42] Introduction of Ga has been decisive in the development of advanced graded bandgap concepts, increasing the bandgap at the surface for boosting the V_{OC}, as well as at the back region for creating an electron reflector, boosting the J_{SC} and fill factor (FF).[43] On the other hand, the use of a postdeposition treatment with heavy alkalis (KF, RbF, or CsF), was shown to enhance the Cu-depletion at the CIGSSe surface, together with their Ga-enrichment, and some likely passivation effect.[35,37,38] All these innovations have introduced in most cases complementary positive effects on CIGSSe absorbers, contributing to boost the efficiency close to 23%. Undoubtedly, this progress is closely related to two types of processes: doping and alloying.

Thus, considering their importance, in the next sections a critical review on the current doping and alloying strategies followed in kesterite will be presented and discussed in the frame of the future perspectives for the efficiency improvement of these technologies. Additionally, accounting for the advantages and limitations of kesterite materials, selected relevant broad technological applications will be discussed in the closing part of this review.

2. Challenges and Perspectives: How to Improve the Kesterite Efficiency?

Motivated by the complexity, tunability, and richness of the kesterite structure, several elements have been tested as dopants and alloying candidates. Considering the Periodic Table of Elements (**Figure 3**), intrinsic doping (i.e., variation of Cu, Zn, and Sn content), extrinsic doping with iso-electronic elements (most commonly with elements coming from the same column than Cu, Zn, and Sn), and extrinsic doping with alkaline elements (Li, Na, K, Rb, and Cs) are so far the most investigated ones. Concerning alloying, cationic substitution using isoelectronic elements from the same column is logically the preferred option, and we can mention the substitution of Cu by Ag, Zn by Cd, and Sn by Ge or Si, although less conventional options such as Mg, Mn, and Fe have been also reported. In the following, we present a review of the solutions for intrinsic and extrinsic doping of kesterite, as well as the alloying strategies followed until now, with the aim to shed light on the origin of the V_{OC} deficit and to provide future pathways addressing this issue.

2.1. Intrinsic Doping

From the early stages of the development of these materials, it has been well known that an off-stoichiometric composition is required to obtain high efficiency devices.[26,44] Particularly, the highest performing devices reported so far have been Cu-poor, Sn-stoichiometric, and Zn-rich composition,[44–46] while Zn-poor[47,48] and/or Cu-rich[48] conditions lead to poor efficiency solar cells. Due to the importance of composition in the conversion efficiency of kesterite, and its intimate relationship with defects and secondary phases formation, Lafond et al.[49] first introduced a classification of compositional-types materials, lately extended by Gurieva et al.[50] as is shown in **Figure 4**. Up to 12 compositional-type kesterites were proposed, each of them corresponding to different cationic balances (combining all possible poor and rich regions for each cation) and including a detailed description of the most probable secondary phases and intrinsic point defects formation.[50,51] As a remarkable property of this material, Valle Rios et al. have shown the flexibility of kesterite-type structure, which can self-adapt from copper-poor up to copper-rich compositions without any structural change except in terms of cation distribution.[52]

But a question remains: why are the highest efficiencies reported so far for kesterite Cu-poor and Zn-rich, and why do their compositions fall very close to the so called "A-line" (corresponding to Cu-poor, Zn-rich, and Sn-stoichiometric composition)?

To shed light on this topic, one must consider the pathways through which kesterite can be formed. It can happen in principle following either a direct reaction of the elements or corresponding alloys, through the binaries (Equation (2)), or including more complex molecules (Equation (3)). The

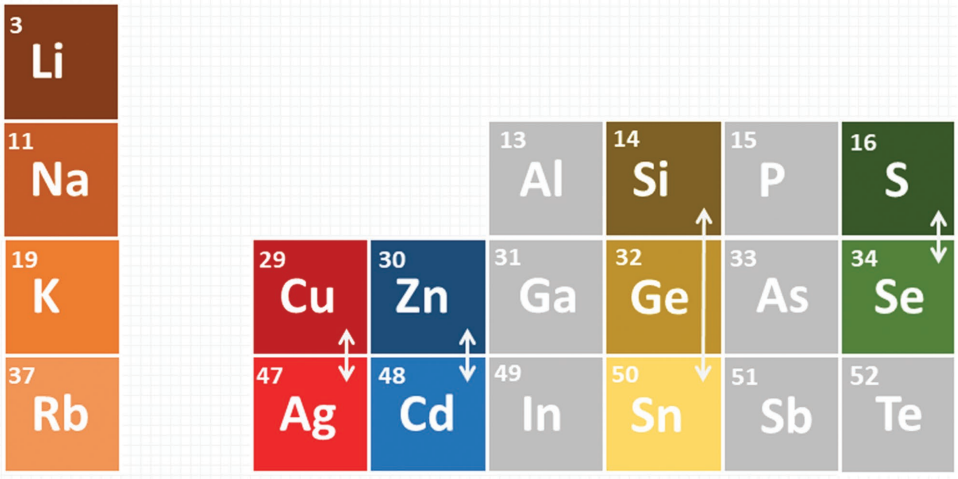

Figure 3. Schematic representation of some sections of the Periodic Table, highlighting the most interesting candidates for doping and alloying in kesterite.

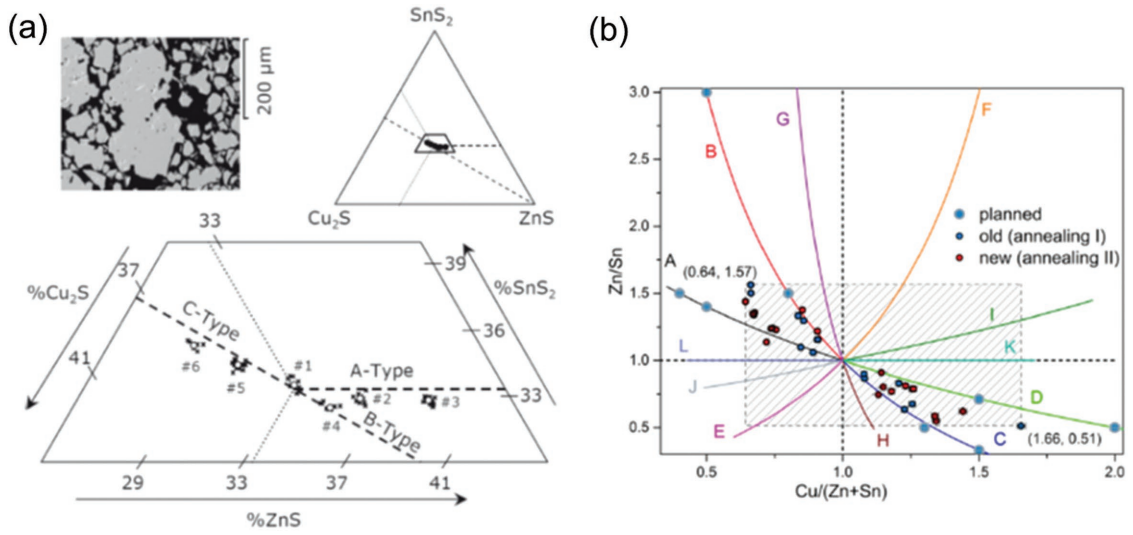

Figure 4. a) First off-stoichiometric types kesterite (A-, B-, and C-type) proposed by Lafond et al. Reproduced with permission.[49] Copyright 2012, Wiley-VCH. b) Complete classification of off-stoichiometric kesterite presented by Gurieva et al. Reproduced with permission.[50] Copyright 2018, Wiley-VCH.

direct reaction of metals with the chalcogen to form kesterite is almost impossible, as at least one binary phase (ZnX, with X = S and Se) is more stable[53] than the quaternary phase, and it is therefore expected that simpler chalcogen species are formed first. Then, kesterite synthesis can proceed via the following equations (where X = S or Se).

$$Cu_2X_{(s)} + ZnX_{(s)} + SnX_{(s)} + 1/2X_{2(g)} \overset{T,p,t}{\leftrightarrow} Cu_2ZnSnX_{4(s)} \quad (2)$$

$$Cu_2SnX_{3(s)} + ZnX_{(s)} \overset{T,p,t}{\leftrightarrow} Cu_2ZnSnX_{4(s)} \quad (3)$$

These last two equations illustrate the most probable pathways followed during the synthesis of kesterite, depending on the temperature and pressure of the system. The first species always formed in this system, irrespectively of the subsequent pathway (Equation (2) or 3), is ZnX due to the high stability of these compounds. After formation of the binary or ternary compounds, ZnX is introduced in the structure forming the kesterite.[15,54] According to this process, one can consider that from the very beginning of the reaction, the kesterite phase is Zn-poor which in return conditions the formation of associated point defects, as will be discussed later. To compensate this detrimental effect, global Zn-rich conditions are required, in order to ensure that the reaction will be fully completed, and to minimize the risk of detrimental Cu–X, Sn–X, or Cu–Sn–X phases remaining unreacted. This is, to the best of our knowledge and understanding, the most likely explanation for the necessity of Zn-rich conditions in the synthesis of high-quality kesterite from an opto-electronic point of view, leading to films nearly free of secondary phases. The further-discussed Cu-poor requisite is more complex, and is strongly related to the formation of intrinsic defects controlling the doping level of the material.[55]

In this sense, and similarly to previous works reported on other chalcogenides, intrinsic doping in kesterite is revealed as very relevant. This was clearly demonstrated by Dimitrievska et al.[56] in a combinatorial experiment where the highest efficiencies are obtained around the previously mentioned A compositional line as shown in **Figure 5**a (in between the B- and L-lines). According to this work, the most probable point defects to be formed are V_{Cu}, Cu_{Zn}, and Zn_{Cu},[51,56] all of them classified as shallow defects[55] (V_{Cu} and Cu_{Zn} are shallow acceptors and Zn_{Cu} a shallow donor), which in principle should have a limited impact on recombination processes. These theoretical predictions are based on stoichiometric material, while all the high-efficiency devices made with kesterite are Cu-poor. This suggests that V_{Cu} could have a preponderant role in the intrinsic doping. Additionally, this case is very similar to that of CIGSSe,[57] where the intrinsic p-doping of the material is also explained by the presence of V_{Cu}. Nevertheless and to the best of our knowledge, no conclusive work on kesterite and the intrinsic doping mechanism has been reported so far, so additional investigations will be required in the future. In this same work, Dimitrievska et al.[56] demonstrated that this compositional regime corresponds to a region where the secondary phase formation in kesterite (at least for the selenide compound) is minimized; in this case, the main possible secondary phase is ZnSe (or ZnS for the case of the sulfide compound), which can be easily detected and removed.[58–63]

In addition to the variety of intrinsic defects due to lattice antisites or vacancies, a second order of complexity is introduced by the fact that Sn can easily adopt two oxidation states: Sn^{+2} and Sn^{+4}. Even if never directly reported, the reduction of Sn^{+4} to Sn^{+2} has been suggested as a possible source of deep defects, and of course as possibly participating in the V_{OC} deficit.[64,65] In fact, recent theoretical calculations suggest that the presence of chalcogen vacancies (S or Se vacancies) can induce the formation of reduced Sn species (Sn^{+3}), introducing a deep defect in the kesterite bands.[66] According to this work, the control of the partial pressure of the chalcogen during the synthesis of kesterite is a crucial parameter to ensure that Sn does not adopt reduced oxidation states. The same authors[66] propose that Sn_{Zn} can be also ascribed as a "killer defect" acting

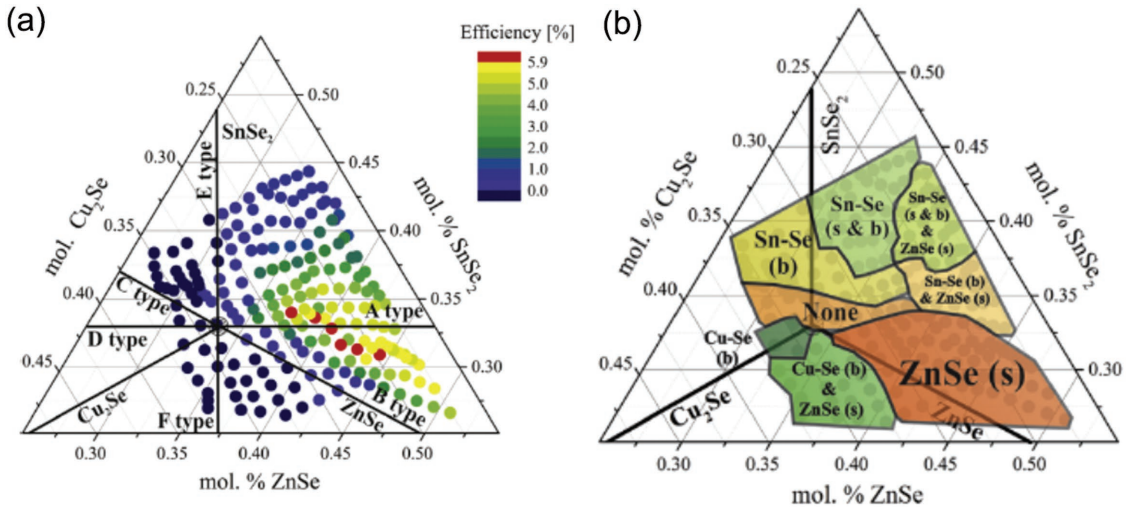

Figure 5. a) Combinatorial experiment showing the relationship of conversion efficiency with composition. b) Secondary phases composition (at the surface) as a function of the kesterite composition. a,b) Reproduced with permission.[56] Copyright 2016, Elsevier.

on electron trapping/detrapping, mainly in the sulfide kesterite compound, and to lesser extent in the selenium one. This seems at first to contradict the fact that all the good performing kesterites are prepared under Zn-rich conditions. However, when taking into account the previous formation process of kesterite previously discussed, one can observe that a Zn-poor kesterite can coexist with Zn-chalcogenide during the synthesis process, then figure out that the presence of a donor Sn_{Zn} defect can in return be compatible with that compositional regime.

Accounting for the previous discussion, we can consider that a quite complete mapping of kesterite composition and its relationship with point defects and secondary phases is now available. The previously discussed studies provide an in-depth analysis of the intrinsic doping solutions in kesterite which is revealed as a key parameter. The optimal absorber composition for high-efficiency devices is found to be somewhere close to the so-called A-line, where less detrimental point defects and fewer secondary phases are being formed. However, although there is nowadays a consensus about the optimum kesterite composition, it remains crucial to ensure the accuracy and the appropriate calibration of the selected method determining the composition. And more importantly, although the composition is fixed during the synthesis process, an increasing number of studies have identified compositional fluctuations at the micro- and nanoscale levels, a possible culprit for electric field and bandgap fluctuations in the material; such observation could partly explain the voltage deficit observed in the material.[67–71] As a result, understanding and controlling the film's homogeneity at different scales nowadays is an urgent issue to address to overcome the current limitations of kesterite-based solar cells.

A final consideration to account is related to the volatility of Sn-chalcogenide species and the resulting possible decomposition of kesterite at relatively high temperatures.[72] During the processing of kesterite, and most probably during the cool-down process as well, it is highly possible that kesterite release Sn to the atmosphere.[73] We can easily figure out selective Sn-loss from the surface, creating Sn-poor conditions and the associated defects. This specific issue will need more thorough investigations in the future.

Considering the previously discussed investigations, we can tentatively identify and propose solutions to address the most problematic defects expected on kesterite, depending on the compositional regime and synthesis conditions. Past experiments show that most of the devices with high efficiency fall into the compositional region defined by the A-, B-, and L-type kesterite.[51] During the processing of the layers, Zn-poor kesterite can occur even at Zn-rich conditions due to the stability of Zn-chalcogenides, promoting the formation of Sn_{Zn} antisites implying the possible reduction of Sn^{+4} to Sn^{+2} among other detrimental effects. Worse, under the presence of low chalcogen availability, sulfur and/or selenium vacancies are prone to be formed which can imply, at least in the case of the sulfur kesterite, the formation of reduced Sn species (Sn^{+3}) potentially acting as an efficient deep electron trap.[66]

A summary of the most probable defects in kesterite is presented in **Table 2**, with a special emphasis highlighting the most detrimental one, i.e., the defects that introduce deep levels in the bandgap. There is unfortunately no available thorough experimental study and characterization of deep defects on kesterite. It is therefore a priority to progress toward the full characterization of deep defects, which can decisively impact future progress of the technology.

2.2. Extrinsic Doping

The complexity of kesterite implies that even in the most favorable cases, intrinsic detrimental defects are expected due to compositional or processing issues. Such defects can in principle be compensated through an adequate design of extrinsic doping, but it remains a challenging task considering that very little is known about deep defects in these materials. Nevertheless, several examples of beneficial extrinsic doping of kesterite exist in the literature, and it has steadily been referred as a "hot

Table 2. Summary of the most probable defects expected in kesterite, depending on the compositional regime and the synthesis conditions. Deep defects are highlighted due to their potential to act as recombination centers, significantly affecting the V_{OC} of the solar cell devices.

Condition	Defects	Comments
A-line Cu-poor, Zn-rich, Sn-stoich.	V_{Cu} and Zn_{Cu}	Both defects are predicted as shallow centers, and in consequence this composition is considered the most benign one.
B-line Cu-poor, Zn-rich, Sn-poor.	Zn_{Cu} and $\mathbf{Zn}_{Sn}$	$\mathbf{Zn}_{Sn}$ can be a relatively deep defect, but in principle this compositional regime can also be considered relatively benign.
L-line Cu-poor, Zn-stoich., Sn-stoich.	Zn_{Cu}, $\mathbf{Sn}_{Cu}$, and V_{Cu}	$\mathbf{Sn}_{Cu}$ can be a deep defect, and compositions close to the L-type kesterite are not recommended.
Overall Zn-poor condition following the phase diagram	$\mathbf{Sn}_{Zn}$ and $\mathbf{Sn}^{+2}$	$\mathbf{Sn}_{Zn}$ and **reduced Sn species** can be very detrimental. Their formation is made possible due to the intrinsic nature of kesterite where Zn-chalcogenides are very stable phases allowing the formation of Zn-poor kesterite even under Zn-rich overall conditions.
Low chalcogen availability	V_X and $\mathbf{Sn}^{+3}$	Depending on the chalcogen availability, there is a possibility to form chalcogen vacancies, which although being benign, can induce the formation of **Sn reduced species** that introduce deep defects.
Sn-loss	$\mathbf{V}_{Sn}$, $\mathbf{Zn}_{Sn}$, and $\mathbf{Cu}_{Sn}$	Due to the intrinsic volatility of Sn-chalcogenides, during slow cool-down processes Sn can be lost at least at the very surface, forming deep $\mathbf{V}_{Sn}$, $\mathbf{Zn}_{Sn}$, and $\mathbf{Cu}_{Sn}$ defects.

topic" of this material. For convenience, a classification in three different types of extrinsic doping is possible:

1. Extrinsic doping with nonconventional elements: In,[74] Bi,[75,76] Sb,[77–80] and Fe[70]
2. Extrinsic doping with isoelectronic elements from the same family as Cu, Zn, and Sn: this includes Ag,[81] Cd,[70,81] and more extensively Ge[15,65,82–87]
3. Extrinsic doping with alkaline elements: Li,[88–92] Na,[58,63,75,77–86 ,93–100] K,[90,91,96,98,101,102] Rb,[90,91] and Cs.[90,91]

The use of "nonconventional elements" has barely been investigated, most probably because their use has demonstrated a limited impact on CIGSSe as well, and only few examples are available in the literature. For instance, kesterite-based cells seem to accept a relatively high quantity of In without affecting much of their properties.[74,103] Giraldo et al.[74] demonstrated that kesterite is resilient to relatively large quantities of In, and the deterioration for large In quantities is associated to the formation of a conductive Sn-In-O phase. Hartnauer et al.[103] also observed that kesterite can accommodate a lot of In, suppressing the presence of ZnSe most probably from the formation of $CuInZn_2Se_4$ phases. This is an important finding since some buffer (In_2S_3)[104–107] and window (In_2O_3:SnO_2, ITO) layers contain In, suggesting that some possible interdiffusion will not have a detrimental influence on the absorber's properties. Sb and Bi have also been studied and demonstrated interesting properties as possible crystallization flux agents, though unfortunately showing detrimental or no impact on the optoelectronic properties of the devices.[75–79] In particular, Sb seems to strongly interact with Na, and under the presence of this codoping, to markedly increase the grain size.[80] Finally, Fe doping was found detrimental to kesterite,[70] limiting the quasi-Fermi level splitting of the devices even for very low concentrations, and in return the V_{OC} of the devices. This highlights the absolute necessity to control Fe contamination in kesterite solar cells prepared onto steel substrates.[96] The limited success with those extrinsic doping has been nevertheless largely improved using more closely related elements.

In general, more conclusive and impacting results have been obtained using extrinsic doping with elements from the same family as Cu, Zn, and Sn. Cu substitution by Ag has been extensively investigated in that regard. Gautam et al.[81] presented a theoretical analysis of Ag doping in CZTS suggesting that a low level substitution leads to a significant disorder suppression on kesterite, though only under Cu-rich and constrained Cu-poor conditions. Additionally, the same authors hypothesized that Ag_{Cu} could form deep acceptor trap states, thus reducing the concentration of Cu vacancies and most probably with an effect on the carrier's concentration level. In contrast, the opposite effect has been reported, where Cherns et al. observed a high level of disorder (large amount of Cu and Ag antisites) in Ag containing crystals.[108] The effect of Ag in the reduction of disorder on kesterite is still debatable, although we must consider that it could be strongly related to the thermal history of the sample.[33] In that sense, additional rigorous studies are required to confirm or discard beneficial effect of Ag onto the kesterite disorder.

Cd doping was also considered by Gautam at al.,[81] suggesting that it could be a detrimental factor by stabilizing the narrower bandgap stannite structure, instead of the kesterite one. These conclusions will also require further experimental analysis and are yet to be validated by other groups in the laboratory. Furthermore, Collord et al.[70] performed a combinatorial experiment studying a wide range of Cd concentration (0–10 000 ppm), eventually observing a benign effect of this dopant. They particularly observed that while Fe immediately deteriorates the quasi-Fermi level splitting of the devices, this parameter seems to be very resilient to the Cd concentration. This was possibly the first proof of concept of the possible potential of Cd for enhancing the voltage deficit in this system, later used in other works.

More recently, some of the extremely positive results of extrinsic doping with isoelectronic elements have been obtained using small quantities of Ge. Giraldo et al. published for the first time the beneficial effect of Ge as dopant in CZTSe,[65] reporting a large efficiency improvement for very small quantities of Ge (below 0.5%, **Figure 6**a),[65] mainly related to a remarkable increase of V_{OC} and FF (Figure 6b).[84] The notable improvements obtained with Ge have been ascribed to several beneficial effects on kesterite; a strong impact on the grain size has been

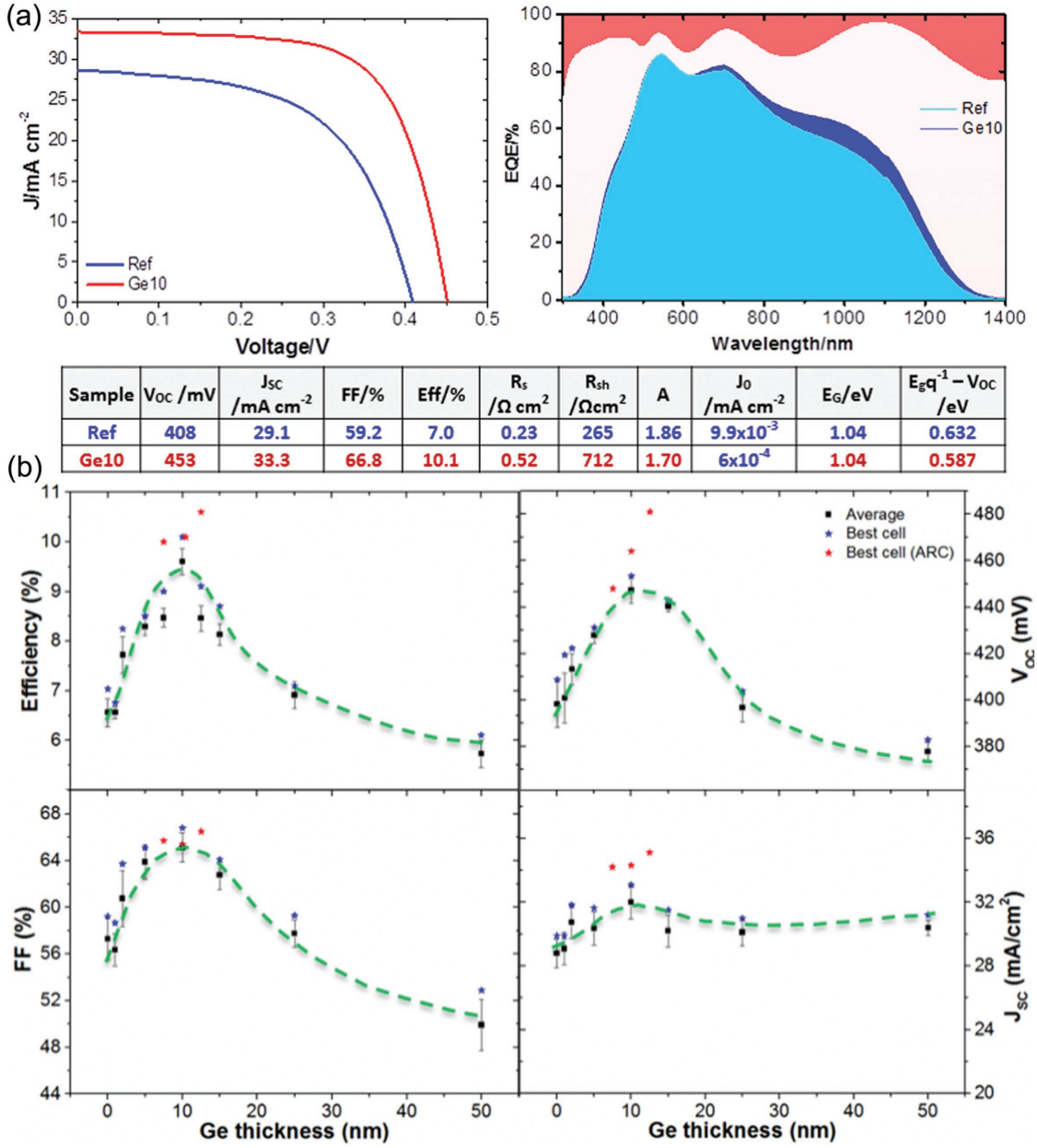

Sample	V_{OC} /mV	J_{SC} /mA cm^{-2}	FF/%	Eff/%	R_s /Ω cm^2	R_{sh} /Ωcm^2	A	J_0 /mA cm^{-2}	E_G/eV	$E_g q^{-1} - V_{OC}$ /eV
Ref	408	29.1	59.2	7.0	0.23	265	1.86	9.9×10^{-3}	1.04	0.632
Ge10	453	33.3	66.8	10.1	0.52	712	1.70	6×10^{-4}	1.04	0.587

Figure 6. a) Efficiency improvement of CZTSe solar cells with very small quantities of Ge. Reproduced with permission.[65] Copyright 2015, Wiley-VCH. b) Effect of Ge doping on the different optoelectronic properties. Reproduced with permission.[84] Copyright 2016, John Wiley and Sons.

observed, and very large grains are frequently obtained.[15,65,84] Giraldo et al. suggested that this is related to the formation of Ge–Se liquid phases at relatively low temperature (380 °C) and acting as crystallization flux.[65] Other beneficial effects of Ge have been reported, including the interaction with Na explaining the impact of this doping element on the carrier's concentration,[82] the modification of the formation pathways that minimize the risk of Sn loss and secondary phases formation,[15] the annihilation or minimization of deep defects,[87] and the passivation of detrimental grain boundary related recombination.[109] By potentially addressing these issues, Ge doping of kesterite contributed to reduce significantly the V_{OC} deficit of CZTSe solar cells to values comparable to those reported for CISe, as was shown in **Table 3**. In that sense, Ge doping shows potential to be one of the most promising pathways to further improve the kesterite solar cells device properties.

Complementary to the last approach, doping with alkaline elements is another strategy that has shown a strong positive impact on kesterite. Li,[88–92] Na,[58,63,75,77–86] K,[90,91,101,102] Rb,[90,91] and Cs[90,91] have been largely studied, and some recent works shed light on the important effect of these dopants. The bulk of this work is inherited from the CIGSSe community, with Na and K having been the first to be investigated. In general, for kesterite, Na was related to an increase in the grain size,[91,96,99] along with a modification of the carrier's concentration.[82,95,100] The mechanisms behind the

Table 3. Compilation of some of the most relevant devices reported in the literature which includes extrinsic doping. The V_{OC} deficit and the V_{OC} gain are included for comparison of the different strategies. N/A: Not Available.

Material	Doping element	E_g[eV]	V_{oc}[mV]	V_{oc} deficit[mV]	V_{oc} gain[mV]	Eff.[%]	Ref.
CZTSe	Na	1.0	423	337	N/A	11.6	[117]
CZTSe	Na	1.07	425	401	17	9.6	[118]
CZTSe	Ge	1.04	453	345	45	10.1	[65]
CZTSe	Ge	1.05	463	344	46	10.0	[82]
CZTSe	Ge	1.05	473	334	72	10.6	[84]
CZTSe	Ge	1.04	463	335	37	11.8	[15]
CZTSSe	Li	1.04	449	349	22	11.8	[88]
CZTSSe	Li	1.11	496	368	N/A	11.5	[91]
CZTSe	K	1.03	350	438	58	5.6	[96]
CZTSe	Na+Ge	1.01	360	409	68	6.1	[96]
CZTSSe	Li	1.08	380	456	70	6.0	[111]
CZTSSe	Rb	1.08	360	476	50	6.4	[111]
CZTSSe	Na	1.12	378	496	68	6.2	[111]
CZTSe	Na	1.05	397	410	N/A	7.5	[98]
CZTSe	In	1.02	423	356	N/A	7.8	[74]
CZTSe	Na	1.0	N/A	N/A	36	N/A	[90]
CZTSe	K	1.0	N/A	N/A	28	N/A	[90]
CZTSe	Na+K	1.0	N/A	N/A	53	8.3	[90]
CZTSe	Na	1.05	409	398	79	7.9	[115]
CZTSe	K	1.05	364	443	34	5.4	[115]
CZTSe	Na+K	1.05	421	386	91	8.3	[115]
CZTS	Na	1.5	628	607	47	6.3	[119]

strong effect on carrier concentration due to Na doping is still unclear, because as Na occupies Cu position in principle, and is iso-electronic to this element, no significant impact on the electric properties is expected. Nevertheless, two possible mechanisms influencing the carrier concentration can be hypothesized. The first is to consider that in most cases, A-type kesterite is used for these studies, resulting in Zn_{Cu} shallow donor defect to be formed.[51] When doping with Na, the alkaline element is naturally positioned in Cu-sites, thus replacing Zn in the Zn_{Cu} defects, then reducing the concentration of shallow donor and increasing consequently the p-type conductivity. The other possible explanation can be hinted to a similar mechanism as in CIGSSe, considering that at the higher temperatures required for the synthesis of kesterite (<500 °C), Na becomes very soluble in the chalcogenide compounds,[110] occupying Cu positions. While during the cooling-down process, Na solubility strongly decreases diffusing toward the grain boundaries, leaving increased number of Cu vacancies. Both mechanisms can be compatible and could very well occur alongside, but the confirmation for either of them is still required.

Additionally, K was also shown to markedly improve the crystalline quality and grain size in kesterite while increasing the carrier's concentration,[91,101,102] yielding results to some extent similar to Na. So far, no specific synergetic behavior was observed between both elements on kesterite.[101] In addition to Na and K, Li was also demonstrated as having a strong impact on kesterite-based device properties. Collord et al. observed a large increase of the conversion efficiency when adding small Li quantities to their molecular ink using DMSO. Main improvements were in the J_{SC} and FF, with a moderate impact on the V_{OC}. In this work, the authors proposed that Li inverts the potential at the grain boundaries to explain the boost in conversion efficiency, but no specific effect of Li on the crystalline properties was observed for this element. However, Yang et al.[92] demonstrated that Li promotes the Na diffusion from the soda lime glass substrate, while being only efficiently incorporated into the kesterite under the absence of Na. Then, for an efficient incorporation of Li Na-free substrates or Na diffusion barriers are required.

Remarkable results were obtained with several elements, and up until recently, no clear consensus existed within the community on which alkaline element constitutes the best option for kesterite extrinsic doping, with different authors proposing their approach to alkalis doping as the optimum one.[90,96,111,112]

This question has been recently solved by Haass et al.,[91] with a study showing the existence of a complex interplay between the different alkaline elements and Sn. As is shown in **Figure 7**, each alkaline element has an optimal associated Sn content in the layer for maximizing the efficiency, evidencing that there is a strong interaction between these elements, similarly to what was observed for Ge and Na.[82] The observed trend was that lighter atoms required higher Sn

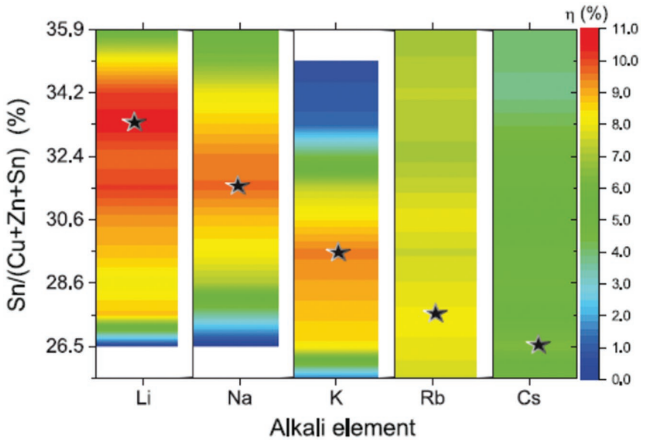

Figure 7. Optimal composition for the different alkali elements in terms of conversion efficiency reported by Haass et al. Reproduced with permission.[91] Copyright 2018, Wiley-VCH.

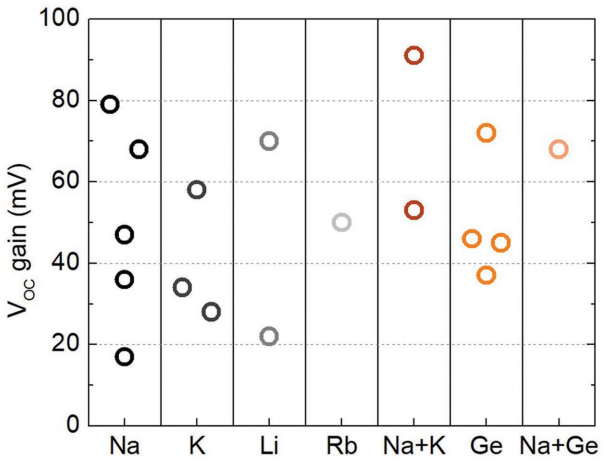

Figure 8. V_{OC} gain for the most relevant extrinsic dopants published for kesterite. The values were extracted from Table 2.

content for maximizing the conversion efficiency. In this specific case, the higher V_{OC} was obtained for Li correlating well with the wider bandgap for the Li-doped samples, while the J_{SC} was maximized by Na and K doping. Overall, Li leads to the highest conversion efficiency and the following order between the alkaline elements as dopants in kesterite was established: Li > Na ≈ K > Rb > Cs.

Overall, very high efficiencies can be obtained from doping with the lighter alkaline elements, nominally Li and Na. The use of one or the other depends on many external parameters such as the type of substrate and the processing method. Currently, the best results obtained with Li are reported for absorber prepared via chemical routes,[88,91] while excellent results were reported with Na doping for absorbers prepared via physical and chemical routes.[15,113,114] The selection of either method thus depends so far on the processes used in each laboratory, also considering that it will be necessary to adjust the Sn content to each specific case. The main improvements are in the V_{OC} of the devices, although the J_{SC} and FF seem to be positively affected. The reasons behind these improvements are still under investigation, but one can mention the impact on the carrier concentration, the improvement of the grain size, the possible interfaces and grain boundaries passivation, and the annihilation of some deep defects as the most plausible explanations.[90,96,115,116]

Finally, as a summary of doping elements on kesterite, Table 3 compiles some of the most relevant contributions to date in this topic, including selected figures of merit illustrating their effect on final photovoltaic devices. The V_{OC} deficit and the V_{OC} gain were particularly shown whenever possible, as they relate in our opinion to the main limitation of kesterite solar cells. In that context, the V_{OC} deficit was calculated as explained in Section 1, whiles the V_{OC} gain represents the magnitude of the voltage that is increased with respect to the reference device, when this value is available. **Figure 8** illustrates the V_{OC} gain for the different dopant elements. Values ranging from 20 mV up to almost 100 mV can be gained when extrinsic doping strategies are implemented in kesterite. Na, Li, Na+K, Ge, and Na+Ge seem to be the most promising dopants to increase the voltage (i.e., decrease the V_{OC} deficit) and are being established as the leading research pathways going forward by the community.

2.3. Alloying

Alloying is the latest strategy introduced to tackle the V_{OC}-deficit issue in kesterite solar cells. Largely used in other thin film PV technologies like CIGSSe or CdTe,[120] it has been a precious asset to tune and improve the properties of these materials, as well as a valuable tool for implementing more advanced devices concepts such as band engineering in the absorber.[121,122] Referring to Figure 3, it is evident that some of the proposed doping elements could also be useful for alloying strategies in kesterite absorbers. More specifically, Ag can substitute Cu, Cd substitutes Zn, and Ge or Si are the ideal candidates for Sn substitution. Beyond these elements, other options have been explored in the literature, including Mg and Mn.

Substitution of Cu by Ag (Ag_2ZnSnS_4, AZTS; $Ag_2ZnSnSe_4$, AZTSe) has been under investigation for some years, with the aim of reducing or eliminating the Cu/Zn disorder problem, thanks to the larger size of Ag atom with respect to Cu. A theoretical study presented by Yuan et al.[123] highlighted the potential of Cu substitution by Ag, predicting that Ag-based kesterite must exhibit either intrinsic or weak n-type conductivity due to the very low concentration of Ag_{Zn} antisite defects, in addition to the fact that the dominant defects are donors, most probably Zn_{Ag}. They proposed that alloying of $Cu_2ZnSn(S,Se)_4$ with Ag can be helpful to overcome the V_{OC} deficit due to a reduction in defect concentration, a conclusion which was further supported by Chagarov et al.,[124] but later contradicted by the work of Cherns et al.[108] Nevertheless, and as was highlighted before, the disorder also strongly depends on the thermal history and composition of the samples, so deeper and complementary studies are required to validate all these results. Additionally, composition-graded $(Cu,Ag)_2ZnSn(S,Se)_4$ alloys provide interesting perspectives in band engineering for boosting the efficiency of kesterite. Following these works, Gershon et al.[125] published a 5% efficient FTO/AZTSe/MoO_3/ITO device, reporting that AZTSe is indeed a n-type semiconductor,

thus agreeing with previous theoretical work,[123] although some recent studies claimed the possibility to obtain p-type AZTS.[126] It was found that when increasing the Ag content on $(Cu_{1-x}Ag_x)_2ZnSn(S,Se)_4$, a compensation effect occurs and reduces the charge carrier density, leading in a change of the conductivity type from p to n for Ag concentrations higher than 50%.[127] Several papers investigated on important properties of these materials, including morphology, bandgap, optimal composition, various electrical properties, and the positive impact on the V_{OC} of the devices, with an estimated 30 mV gain[128–130] with respect to the alloys with equivalent bandgap. In particular, AZTS exhibits larger grains, higher mobility, and a lower carrier density than the corresponding Cu counterpart.[128] Additionally, the material seems to yield better performances under higher Ag/Sn ratios than the Cu alloy, correlating well with the lower doping level normally observed in these alloys and contributing to the conductivity type change.[129]

Due to the possible n-type and large band-offset with CdS,[131] ACZTS(Se) has been investigated as n-type layer in CZTS/AZTS heterojunctions leading to an encouraging 4.5% efficiency,[132] with even a p-type AZTS/n-type AZTS homojunction being later considered, though with a more limited 0.9% efficiency reported so far.[133] These preliminary approaches are not without future, as a recently published theoretical work proposed a CdS/ACZTS/CZTS (n/p/p+) solar cell with a potential efficiency close to 20%,[134] but no experimental demonstration was made up to date. Nevertheless, the latest progress using solution-processed $(Cu_{1-x}Ag_x)_2ZnSn(S,Se)_4$ with 3% of Ag (with respect to Cu) has reported a 10.4% efficiency,[135] and 10.2% using co-evaporation for the pure selenide compound with up to 10% of Ag,[127] hence revitalizing the interest in the Ag-based kesterite alloys and paving the way toward future improvements. The key issue for the future is to keep the Ag concentration well below 50% in order to ensure that the absorber remains p-type, and no radical changes in the solar cell structure are required. Otherwise, concentrations higher than 50% will require a complete revisiting of the heterostructure to accommodate a homojunction or an n-type absorber.

Another possible alloying being considered is cationic substitution using Cd to replace Zn. Once again the main objective is reducing the Cu/Zn disorder by introducing a bigger atom in the structure, although theoretical DFT calculations suggested that the formation energy of Cu_{Cd} antisite is very similar to the case of Cu_{Zn}, and then no remarkable impact on the lattice order is expected.[123] Additionally, Cd interest is limited to the case of the sulfide compound as Cd alloying lowers the bandgap of the corresponding compounds, rendering the case of selenide kesterite well below the optimum bandgap value. Asides from toxicity considerations accompanying the use of a large amount of Cd, an early work from Xiao et al. studied the $Cu_2(Zn,Cd)SnS_4$ (CZCTS) compound,[136] demonstrating the possibility to finely tune the bandgap between 1.09 and 1.55 eV and obtaining a first proof of concept yielding 1.2% efficiency (for a Cd content of 0.47). These results were further supported by Pilvet et al. in monograin CZCTS absorbers with tuned composition.[137] Complementary results were reported by Zhang et al.[138] for a kesterite–stannite structure transition at 50% of Cd content, showing a remarkably increased grain size for such high Cd content in the alloy, and a narrower bandgap range of 1.35–1.15 eV as compared to previous papers. Meng et al.[139] later obtained an improvement in the solar cell performances by modifying the back contact with a Cd layer, while further improvement in the absorber synthesis and solar cells fabrication led to Su et al. reporting a 9.2% efficiency device with 40% of Cd.[140] The key reason for such drastic improvements in such a short timeframe is the fine optimization of the Zn/Cd ratio, which contributes greatly to enhance the grain size while also reducing the quantity of detrimental ZnS secondary phases. A transition from kesterite to stannite structure was observed albeit limited to Cd content higher than 60%. Other recent progress reported by Yan et al.[141] demonstrated that Cd-alloying reduces the band tailing effect, thus improving the microstructure, minority carrier lifetime, and electrical properties in general, and a champion cell over 11% efficiency was achieved, very close to the state of the art of standard CZTSSe solar cells. Moreover, it was very recently reported that the introduction of Cd could improve the solar cell devices performances by altering the characteristics of acceptor defects near the valence band, specifically by making them shallower.[142] This swift progress positioned Cd alloying as a very promising route for boosting the V_{OC} deficit of kesterite, and it could even be used in the future to implement advanced bandgap grading concepts.

The latest important substitution strategy worth mentioning is the introduction of Ge replacing Sn. Even if Ge is considered a CRM, the use of this element by partial substitution can be sustainable. For example, if Sn is substituted by 20% of Ge, we estimate that less than 1 Ton of Ge will be required to produce 1 GW for a solar panel with 15% efficiency. This represents less than 1% of the total Ge produced in the world. Nevertheless, it will be interesting to reduce as much as possible the use of Ge in kesterite technology. From the very beginning, and as in the case of Ge-doping,[15] Ge-alloying (Cu_2ZnGeS_4, CZGS; $Cu_2ZnGeSe_4$, CZGSe) has demonstrated an extremely positive impact on kesterite absorbers. Hages et al.[64] first optimized the Ge containing absorbers for the sulfur–selenide compound, obtaining a remarkable 9.4% efficiency device with 30% of Ge (with respect to Sn), representing a 1% absolute increase as compared to the absorber without Ge, linked to a direct improvement of the V_{OC}. An important increase in the minority carrier lifetime was also observed, establishing Ge as one of the most promising ways to boost the efficiency in kesterite-based solar cells. Progress was steadily made following this initial work, and Kim et al.[143] published a device with over 10% efficiency with a higher Ge content (39%), by optimizing the annealing process. Later on, Collord and Hillhouse[144] reported on the preparation of a continuously graded sample with combinatorial mixing of Ge and Sn containing inks, covering almost the full range of possible Ge/(Sn+Ge) compositional ratios, and obtaining an 11% efficiency device with an optimized 25% content of Ge and a remarkable V_{OC}-deficit reduction. Further Ge concentration increase results in a drastic drop of the conversion efficiency from both an unfavorable band alignment between the kesterite containing Ge and CdS, and the formation of a deep defect located about 0.8 eV above the valence band moving toward mid-gap as the band gap increases with the Ge content. Lastly, Kim et al.[145] further optimized the Ge depth composition, increasing the efficiency up to 12.3%, a

Table 4. Compilation of some of the most relevant devices reported in the literature which includes alloying with Ge, Cd, and Ag.

Material	Alloying element	E_g[eV]	V_{OC}[mV]	V_{OC} deficit[mV]	Eff.[%]	Ref.
CZTGSe	Ge/(Ge+Sn) = 22%	1.11	527	337	12.3	[145]
CZTGSSe	Ge/(Ge+Sn) = 25%	1.2	583	367	11.0	[144]
CZCTS	Cd/(Cd+Zn) = 40%	1.38	650	470	11.5	[141]
CZCTS	Cd/(Cd+Zn) = 40%	1.36	581	521	9.2	[140]
ACZTSSe	Ag/(Ag+Cu) = 3%	1.07	448	378	10.4	[135]
ACZTSe	Ag/(Ag+Cu) = 10%	1.0	423	337	10.2	[127]
ACZCTS	Ag/(Ag+Cu) = 5% Cd/(Cd+Zn) = 25%	1.4	650	490	10.8	[142]

value nearly matching the kesterite world record at that time and with a remarkable improvement of the V_{OC} deficit. This improvement was found to be related to the reduction of band tailing via the control of the Ge/(Sn + Ge) ratio. Additionally, the authors reported a remarkably high FF (73%), suggesting a strong reduction in carrier recombination at the absorber/buffer interface and/or in the space charge region. An improvement on carrier's lifetime was also reported, suggesting an overall higher absorber quality.

The fast progress of the conversion efficiency of Ge-alloyed kesterite positions it as one of the most promising ways to improve the conversion efficiency. In fact, very recent results from Gunder et al.[146] demonstrated that CZGSe also exhibits kesterite structure, and the more detrimental Cu_{Ge} defect is only formed in the stoichiometric or Cu-rich compound, but does not appear preponderant in the Cu-poor devices reported in the literature.

Following the fast progress of Ge-alloying, a pure CZGSe solar cell has recently been published yielding 7.6% efficiency, thanks to the optimization of the buffer layer,[147] and with a V_{OC} of 558 mV. Yet, the V_{OC} on these devices seems to be mostly limited by the interface recombination due to the nonoptimal band alignment between the absorber and the CdS, giving insights for future improvements using alternative buffer layers. Finally, very recent results from Marquez et al.,[86] using combined in situ energy-dispersive X-ray diffraction (EDXRD) synchrotron measurements and high-resolution scanning electron microscopy/energy-dispersive X-ray spectroscopy (SEM/EDX) characterization, have shown that Ge tends to accumulate toward the back contact in Sn–Ge alloys, similarly to Ga in CIGSSe, opening opportunities for back contact interface management in the future (back surface field, improved contact ohmicity).

As a summary of this section, the most relevant results obtained until now for the three different alloying approaches are outlined in **Table 4**, highlighting the potential to further develop these strategies promising improvements in the conversion efficiency of kesterite-based solar cells.

Other elements have been tested for alloying such as Mn,[148,149] Mg,[150] and Fe[151] with device performances still at the 7–8% level and using very low concentration for Mn and Mg (less than 5%), or 2–3% efficiency with the total substation of Zn by Fe. For the moment, these substitutions are still not competitive with the previously presented ones.

While steady advances in the description of the intrinsic characteristics of kesterite have been made, and the investigations and progress obtained studying extrinsic doping and alloying are extremely valuable assets going forward, kesterite still suffers from a large V_{OC} deficit. As the fundamental understanding of this material is improving each year, the opinion of the authors is that underlying issues continue hindering the technology and should be addressed in the briefest delay by the community. Namely, deep defects, band tailing, inhomogeneities, and interface recombination are considered of high relevance and are summarized in **Table 5**. The table also includes some possible technological solutions which we require thorough investigation as promising pathways to boost the V_{OC} and concomitantly the conversion efficiency.

3. Future Technological Applications

With a record efficiency of 13%,[24] kesterite-based solar cells may still be considered as too upstream to yet contemplate direct applications of the technology. However, this is to some extent a misconception as even with this level of performance, an earth abundant and reliable technology is a pertinent addition to the mix of thin film materials available for various fields of application.

Combining thin film solar cells with crystalline silicon is seen as a straightforward and relatively low-cost way to markedly increase the efficiency of a technology currently so close to the Shockley–Queisser limit that very limited improvements are to be expected in the upcoming years. As mentioned before, CZTSSe-based solar cells seem to be less sensitive to voltage deficit at high bandgaps than their currently more efficient counterparts (see Figure 2b). Efficiencies above to 10% have been achieved for bandgap above 1.5 eV,[152] which makes kesterite photovoltaics a serious contender for top cell application in a tandem device with crystalline silicon. We also reported bifacial kesterite solar cells grown on fluorine-doped tin oxide (FTO) substrate,[153] with efficiencies close to 8% thanks to the insertion of a semitransparent Mo nanolayer at the back interface, showcasing the adaptability of CZTSSe technology. Recent in-house modeling (**Figure 9**, top left) showed that for bandgaps ranging from 1.5 to 1.9 eV, a theoretical tandem device would overcome the base efficiency of a single c-Si cell by a significant margin for a top cell efficiency above 13%, a value not that far off from current performances at similar bandgaps and within direct reach of future optimizations. Indeed, recent progress has been made for wide bandgap/sulfur content kesterite cells, with the V_{oc} deficit partly resorted thanks to the introduction of a high work function material at the back interface using a

Table 5. Most probable origins for the V_{OC} deficit of kesterite, and proposed technological solutions to be applied and investigated in the future

Possible reasons of the V_{OC} deficit	Possible origin	Proposed technological solution
Deep defects related to Sn: • Sn_{Zn} • Sn vacancies • Sn reduced species	• Zn-poor absorber due to the high stability of Zn-chalcogenides • Sn-chalcogenide volatile species • Formation of chalcogen vacancies	• Substitution of Sn by Ge • Substitution of Zn by atoms forming less stable compounds with chalcogens (Cd, Mn, Mg, Ba, etc.) • Postdeposition treatments under Sn containing atmosphere ($SnCl_4$, $SnS(Se)_2$, SnF_4) • Postdeposition treatments under Zn containing atmosphere ($ZnCl_2$, ZnI_2) • Postdeposition treatments under Ge containing atmosphere ($GeCl_4$, $GeS(Se)_2$, GeF_4)
Deep defects related to Zn: • Zn_{Sn}	• Zn-rich absorbers • Sn-chalcogenide volatile species	• Substitution of Zn by atoms forming less stable compounds with chalcogens (Cd, Mn, Mg, Ba, etc.) • Postdeposition treatments under Sn containing atmosphere ($SnCl_4$, $SnS(Se)_2$, SnF_4) • Postdeposition treatments under Ge containing atmosphere ($GeCl_4$, $GeS(Se)_2$, GeF_4)
Band tailings due to Cu-Zn disorder	• Zn and Cu isoelectronic elements	• Substitution of Cu by Ag • Substitution of Zn by Cd, Mn, Mg, Ba, etc.
Bulk in-homogeneities	• Zn-chalcogenide high stability • Sn-chalcogenide volatile species that modify the composition of the absorber during the annealing • Precursors formed during the kesterite formation pathway	• Substitution of Zn by Cd, Mn, Mg, or Ba • Substitution of Sn by Ge • Implementation of a very efficient crystallization flux
Interface recombination	• Sn-chalcogenide volatility changes the surface composition during last stages of the annealing process • Mo/kesterite interface instability	• Postdeposition treatments under Sn containing atmosphere ($SnCl_4$, $SnS(Se)_2$, SnF_4) • Postdeposition treatments under Ge containing atmosphere ($GeCl_4$, $GeS(Se)_2$, GeF_4) • Deep coating in Sn or Ge containing solutions and further thermal annealing • Development of efficient intermediate layers between Mo and kesterite

simple lift-off technique,[154] going more recently even further thanks to a specific heat treatment reducing the recombination at the heterojunction.[152] An optimum bandgap of about 1.7 eV was found in our model, which aligns well with previous results from the literature considering similar designs.[155,156] These values are compatible with the high degree of tunability of kesterite materials, as shown by recent results demonstrating that the bandgap could be pushed all the way up to 2 eV with the inclusion of Ge in the compound.[157] And beyond the top cell application in tandem with c-Si, CZTSe films have shown great promise in monolithic integration as a bottom cell with a perovskite top cell, outperforming every other monolithic tandem chalcogenide device including CIGSSe at that time.[158]

Furthermore, the potential of CZTSSe-based photocatalysis has recently been investigated by our group,[159] and an efficient kesterite-based photo-electrochemical water splitting device was realized with extremely encouraging results. The CZTSSe cell was proved resilient to a low temperature protective, transparent and conductive TiO_2 layer synthesized by atomic layer deposition at 200 °C. Through an adjustment of the bandgap by modifying the S/Se ratio, a solar to hydrogen efficiency of up to 7% was obtained, with the potential to go much higher if the stability of the CZTSSe film can be improved for higher S content, as the 200 °C step was so far the limiting factor. A schematic representation of the complete device is shown in Figure 9 (top middle).

The high absorption coefficient (up to 10^5 cm^{-1}) and the wide bandgap tunability of kesterite materials make them an interesting and ecofriendly alternative in the photodetector field.[160] Na doping of CZTS films was found critical to lower the response rise time in a photodetector setup and broadband improvements were observed from visible to near-infrared (NIR) range with roughly 1 order of magnitude improvement across the board.[161,162] Similarly, a very large increase of the photocurrent response was observed, with an almost 2 orders of magnitude improvement. More recently, the increased absorption provided by nanostructuration was found to further decrease the rise and decay time constants.[163] A broadband spectral response in the visible and NIR range was also detected under zero bias conditions, paving the way for self-powered photodetectors based on CZTSSe thin films. An example of *J–V* curve and device scheme are shown in Figure 9 (top right).

Thermoelectric (TE) devices have gained an increasing attention in the past years as a straightforward and reliable way to harvest heat wastes in the form of electric energy (Figure 9, bottom left). While a significant body of work has been done in the previous years on thermoelectric materials, most of them contain rare earth elements as well as tellurium or antimony, and are therefore constrained by natural resources, toxicity, and raw materials cost.[164] In that regard and similarly to the case of solar cells, CZTSSe is an attractive material that has been considered by several groups as an environmentally friendly alternative. CZTS colloidal nanocrystals for TE applications have been reported by Yang et al.[164] and their TE properties analyzed with temperatures ranging from 300 to 700 K. Nanostructuration as well as extra Cu doping were found as critical parameters to enhance the Seebeck coefficient way above that of state-of-the-art

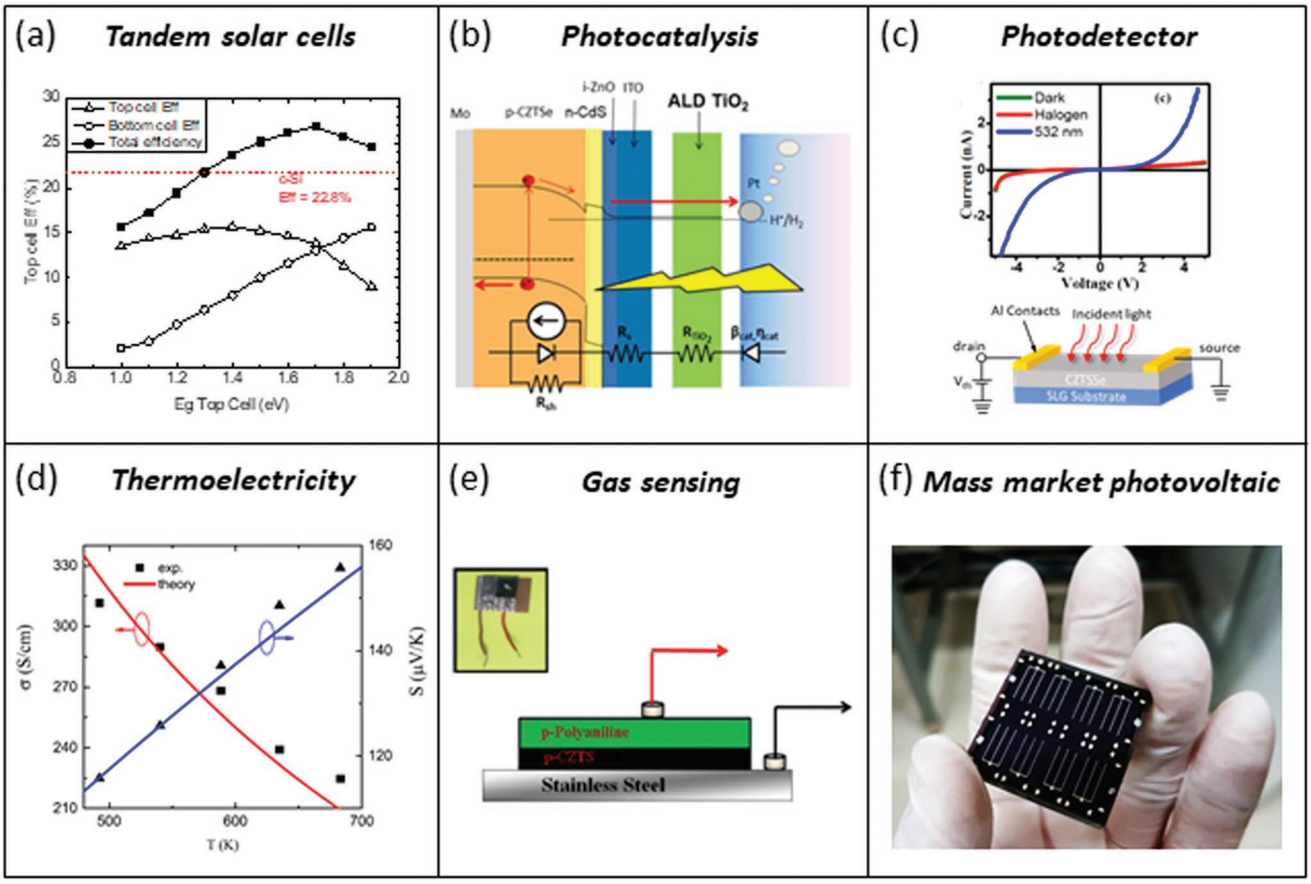

Figure 9. Summary of some relevant technological applications for which kesterite has been proposed. a) Tandem solar cells: modeling of the potential efficiency of a tandem device combining a $Cu_2Zn(Sn,Ge)(S,Se)_4$ cell with a state of the art c-Si cell [authors unpublished results]. b) Photocatalysis: scheme of a CZTSe based PEC water splitting device. A solar to hydrogen conversion efficiency of 7% was already demonstrated. b) Reproduced with permission.[159] Copyright 2018, American Chemical Society. c) Photodetector: *J–V* curve and scheme representation of a CZTSSe photodetector. Reproduced with permission.[162] Copyright 2016, Elsevier B.V. d) Thermoelectricity: comparison of theoretical and experimental thermal conductivity and Seebeck coefficient of CZTSe as a function of temperature. Reproduced with permission.[169] Copyright 2017, American Physical Society. e) Gas sensing: Polyaniline/CZTS heterostructure for gas sensing applications. Reproduced with permission.[171] Copyright 2012, Elsevier B.V. f) Mass market photovoltaic: As previously mentioned, CZTS technology evolves at a rate comparable to CIGS. Recent developments give hope for efficiencies nearing 20% within a decade.

bulk material, thus positioning CZTS as a serious contender for high-temperature thermoelectric energy harvesting. Several studies reported that the thermoelectric properties of CZTSSe nanoparticles were markedly enhanced when increasing the measurement temperature[165–167] although stability issues were reported above 550 °C.[168] Recent first principle theoretical calculations[169] have shown Se-based compounds to be potentially more efficient than S-based compounds, with an optimal hole concentration of 5.10^{19} cm^{-3}, that is significantly higher than the values reported for solar cell applications.

While still a marginal application, CZTSSe films are also considered as an alternative to conductive polymers for efficient and nontoxic gas-sensing devices, in heterostructures with ZnO[170] and polyaniline.[171] Specifically, CZTS-based devices presented a high selectivity in discriminating between O_2, N_2, and liquefied petroleum gas (LPG), as sensible changes in the *J–V* curves were observed in presence of these compounds at room temperature.[171] These devices also exhibited a fast response and recovery time (70 and 40 s, respectively), as well as demonstrating a good stability over time.[170] An illustration of a gas-sensing device from reference[171] based on CZTS is shown in Figure 9 (bottom middle).

Finally, as previously mentioned in this review, kesterite-based solar cells for standard application still hold several advantages in nontoxicity, stability, and sustainability over other technologies which should not be overshadowed; additionally, progress in the conversion efficiencies is still being made and the trend shown in Figure 1 gives hope for the 20% mark to be reached within less than a decade. Moreover, the expertise acquired in the large-scale development of CIGSSe will certainly prove valuable in the long run as both technologies share similar industrial requirements and processes.

4. Conclusions

Among the available emerging thin film photovoltaic technologies based on inorganic compounds, free of critical raw materials and with low toxicity, kesterite appears as the most realistic and promising option. Although the record conversion

efficiency has seen limited improvements in the last 3–4 years, recent progress in the fundamental understanding of the material, and the development of processes and strategies specifically for this class of compounds helped maintain kesterites in a competitive position. The consolidation of reliable technologies in several groups around the world has permitted the development of various parallel strategies to try overcoming the V_{oc} deficit in the solar cells devices, currently the most important technological lock to address. Similarly to chalcopyrite a few years ago, doping and alloying strategies in kesterite have become a key subject destined to be increasingly investigated in the near future. Advances in doping have demonstrated the importance of alkaline doping, with the best results obtained for Li, along with Na and K also showing promising improvements in the performance. Extrinsic and intrinsic doping allowed general advancement in the technology, rendering the current process more reliable and resilient. The extension toward alloying approaches, including the study of new compounds containing Ag in substitution of Cu, Cd in substitution of Zn, and Ge in substitution of Sn, has brought new opportunities to the development of more advanced concepts with kesterite, allowing to tune the optical and electrical properties of the material "a la carte." All this contributes to lay the foundation and raise new interest in kesterite, by studying innovative doping elements and processes, innovative alloying compounds, and applying them into advanced concepts like graded bandgap absorbers for high-efficiency solar cells. After analyzing part of the most relevant literature available for this type of materials, the presence of deep defects not identified yet, the nonhomogeneities at micro- and macroscale, and the presence of interface recombination are identified as the most serious problems to be investigated with urgency. Finally, and even with the state of the art, kesterite continues being relevant and of high interest for several current technological applications beyond conventional photovoltaic devices, demonstrating good performance as possible candidate in advanced tandem concepts, photocatalysis, thermoelectric, gas sensing, etc. Considering the currently limited maturity of this technology, and the complexity of kesterite, it is a matter of time before new breakthroughs in this fascinating family of materials accelerate once again in the race toward high-efficiency solar cells, and some ideas for possible breakthrough have been presented in this review.

Acknowledgements

This research was supported by the H2020 Programme under the projects STARCELL (H2020-NMBP-03-2016-720907) and INFINITE-CELL (H2020-MSCA-RISE-2017-777968), by the Spanish Ministry of Science, Innovation and Universities under the IGNITE (ENE2017-87671-C3-1-R) and WINCOST (ENE2016-80788-C5-1-R), and by the European Regional Development Funds (ERDF, FEDER Programa Competitivitat de Catalunya 2007–2013). Authors from IREC and the University of Barcelona belong to the SEMS (Solar Energy Materials and Systems) Consolidated Research Group of the "Generalitat de Catalunya" (Ref. 2017 SGR 862). S.G. thanks the Government of Spain for the FPI fellowship (BES-2014-068533), M.P. for the Ramon y Cajal Fellowship (RYC-2017-23758), and Z.J. for the TECNIOspring PLUS Fellowship CLEARSUN. E.S. thanks the STARCELL and INFINITE-CELL consortiums for their continuous support.

Conflict of Interest

The authors declare no conflict of interest.

Keywords

alloying, critical raw materials, $Cu_2ZnSn(S,Se)_4$, doping, kesterite, thin film solar cells

Received: October 15, 2018
Revised: December 18, 2018
Published online: February 14, 2019

[1] "Communication from the Commission to the European Parliament, the Council, the European Economic and Social Committee and the Committee of the Regions on the 2017 list of Critical Raw Materials for the EU," http://eur-lex.europa.eu/legal-content/EN/ALL/?uri=COM:2017:0490:FIN (accessed: 2017).
[2] C. Wadia, A. P. Alivisatos, D. M. Kammen, R. Group, S. Division, L. Berkeley, *Environ. Sci. Technol.* **2009**, *43*, 2072.
[3] B. A. Andersson, *Prog. Photovoltaics* **2000**, *8*, 61.
[4] A. Zuser, H. Rechberger, *Resour., Conserv. Recycl.* **2011**, *56*, 56.
[5] V. Fthenakis, *Renewable Sustainable Energy Rev.* **2009**, *13*, 2746.
[6] A. Zakutayev, *Curr. Opin. Green Sustainable Chem.* **2017**, *4*, 8.
[7] T. K. Todorov, S. Singh, D. M. Bishop, O. Gunawan, Y. S. Lee, T. S. Gershon, K. W. Brew, P. D. Antunez, R. Haight, *Nat. Commun.* **2017**, *8*, 682.
[8] R. B. Hall, R. W. Birkmire, J. E. Phillips, J. D. Meaking, *Appl. Phys. Lett.* **1981**, *38*, 925.
[9] T. M. T. Minami, Y. Nishi, *Appl. Phys. Express* **2016**, *9*, 052301.
[10] L. P. Sinsermsuksakul, S. W. Sun, H. H. Lee, S. B. Park, C. Kim, R. G. Yang, *Adv. Energy Mater.* **2014**, *4*, 1400496.
[11] H. T. A. Ennaoui, S. Fiechter, Ch. Pettenkofer, N. Alonso-Vante, K. Büker, M. Bronold, C. Höpfner, *Solar Energy Mater. Solar Cells* **1993**, *29*, 289.
[12] A. C. M. Bhushan, *Appl. Phys. Lett.* **1981**, *38*, 39.
[13] J. Hernádez-Mota, M. Espíndola-Rodríguez, Y. Sánchez, I. López, Y. Peña, E. Saucedo, *Mater. Sci. Semicond. Process.* **2018**, *87*, 37.
[14] A. Kanai, K. Toyonaga, K. Chino, H. Katagiri, H. Araki, *Jpn. J. Appl. Phys.* **2015**, *54*, 08KC06.
[15] S. Giraldo, E. Saucedo, M. Neuschitzer, F. Oliva, M. Placidi, X. Alcobé, V. Izquierdo-Roca, S. Kim, H. Tampo, H. Shibata, A. Perez-Rodriguez, P. Pistor, *Energy Environ. Sci.* **2018**, *11*, 582.
[16] C. Yan, J. Huang, K. Sun, S. Johnston, Y. Zhang, H. Sun, A. Pu, M. He, F. Liu, K. Eder, L. Yang, J. M. Cairney, N. J. Ekins-Daukes, Z. Hameiri, J. A. Stride, S. Chen, M. A. Green, X. Hao, *Nat. Energy* **2018**, *3*, 764.
[17] W. Wang, M. T. Winkler, O. Gunawan, T. Gokmen, T. K. Todorov, Y. Zhu, D. B. Mitzi, *Adv. Energy Mater.* **2014**, *4*, 1301465.
[18] D. Shin, T. Zhu, X. Huang, O. Gunawan, V. Blum, D. B. Mitzi, *Adv. Mater.* **2017**, *29*, 1.
[19] V. Bermudez; A. Perez-Rodriguez, *Nat. Energy* **2018**, *3*, 466.
[20] S. Schorr, M. Tovar, H. J. Hoebler, H. W. Schock, *Thin Solid Films* **2009**, *517*, 2508.
[21] S. Chen, X. G. Gong, A. Walsh, S. H. Wei, *Appl. Phys. Lett.* **2009**, *94*, 25.
[22] S. Siebentritt, S. Schorr, *Prog. Photovoltaics* **2012**, *20*, 512.
[23] T. K. Todorov, K. B. Reuter, D. B. Mitzi, *Adv. Mater.* **2010**, *22*, E156.
[24] D.-H. Son, S.-Y. Kim, S.-H. Kim, Y.-I. Kim, S.-N. Park, D.-H. Jeon, D.-K. Hwang, K.-J. Yang, J.-K. Kang, D.-H. Kim, in *9th European Kesterite Workshop*, Ghent, Belgium **2018**.

[25] L. L. Kazmerski, F. R. White, M. S. Ayyagari, Y. J. Juang, R. P. Patterson, *J. Vac. Sci. Technol.* **1977**, *14*, 65.
[26] H. Katagiri, N. Sasaguchi, S. Hando, S. Hoshino, J. Ohashi, T. Yokota, *Sol. Energy Mater. Sol. Cells* **1997**, *49*, 407.
[27] W. Shockley, H. J. Queisser, *J. Appl. Phys.* **1961**, *32*, 510.
[28] R. Carron, C. Andres, E. Avancini, T. Feurer, S. Nishiwaki, S. Pisoni, F. Fu, M. Lingg, Y. E. Romanyuk, S. Buecheler, A. N. Tiwari, *Thin Solid Films* **2019**, *669*, 482.
[29] J. A. M. Abushama, S. Johnston, T. Moriarty, G. Teeter, K. Ramanathan, R. Noufi, *Prog. Photovoltaics* **2004**, *12*, 39.
[30] Y. Hishikawa, E. D. Dunlop, M. A. Green, J. Hohl, E. Anita, W. Y. H. Baillie, D. H. Levi, *Prog. Photovoltaics* **2018**, *26*, 427.
[31] D. Braunger, D. Hariskos, T. Walter, H. W. Schock, *Sol. Energy Mater. Sol. Cells* **1996**, *40*, 97.
[32] M. A. Contreras, L. M. Mansfield, B. Egaas, J. Li, M. Romero, R. Noufi, E. Rudiger-Voigt, W. Mannstadt, *Prog. Photovoltaics* **2012**, *20*, 843.
[33] G. Bourdais, S. Choné, C. Delatouche, B. Jacob, A. Larramona, G. Moisan, C. Lafond, A. Donatini, F. Rey, G. Siebentritt, S. Walsh, A. Dennler, *Adv. Energy Mater.* **2016**, *6*, 1502276.
[34] C. J. Hages, A. Redinger, S. Levcenko, H. Hempel, M. J. Koeper, R. Agrawal, D. Greiner, C. A. Kaufmann, T. Unold, *Adv. Energy Mater.* **2017**, *7*, 1700167.
[35] Y. Sun, S. Lin, W. Li, S. Cheng, Y. Zhang, Y. Liu, W. Liu, *Engineering* **2017**, *3*, 452.
[36] W. E. Devaney, W. S. Chen, J. M. Stewart, *IEEE Trans. Electron Devices* **1990**, *37*, 428.
[37] A. Chirilă, P. Reinhard, F. Pianezzi, P. Bloesch, A. R. Uhl, C. Fella, L. Kranz, D. Keller, C. Gretener, H. Hagendorfer, D. Jaeger, R. Erni, S. Nishiwaki, S. Buecheler, A. N. Tiwari, *Nat. Mater.* **2013**, *12*, 1107.
[38] P. Jackson, R. Wuerz, D. Hariskos, E. Lotter, W. Witte, M. Powalla, *Phys. Status Solidi RRL* **2016**, *10*, 583.
[39] D. Rudmann, D. Brémaud, H. Zogg, A. N. Tiwari, *J. Appl. Phys.* **2005**, *97*, 084903.
[40] B. L. Kronik, D. Cahen, H. W. Schock, *Adv. Mater.* **1998**, *10*, 31.
[41] Z. Laghfour, S. Aazou, M. Taibi, G. Schmerber, A. Ulyashin, A. Dinia, A. Slaoui, M. Abd-Lefdil, Z. Sekkat, *Superlattices Microstruct.* **2018**, *120*, 747.
[42] R. Mainz, E. Simsek Sanli, H. Stange, D. Azulay, S. Brunken, D. Greiner, S. Hajaj, M. D. Heinemann, C. A. Kaufmann, M. Klaus, Q. M. Ramasse, H. Rodriguez-Alvarez, A. Weber, I. Balberg, O. Millo, P. A. van Aken, D. Abou-Ras, *Energy Environ. Sci.* **2016**, *9*, 1818.
[43] T. Nakada, Y. Hirabayashi, T. Tokado, D. Ohmori, T. Mise, *Sol. Energy* **2004**, *77*, 739.
[44] S. Delbos, *EPJ Photovoltaics* **2012**, *3*, 35004.
[45] J. Márquez, M. Neuschitzer, M. Dimitrievska, R. Gunder, S. Haass, M. Werner, Y. E. Romanyuk, S. Schorr, N. M. Pearsall, I. Forbes, *Sol. Energy Mater. Sol. Cells* **2016**, *144*, 579.
[46] F. A. Pulgarín-Agudelo, O. Vigil-Galán, J. A. Andrade-Arvizu, J. R. González-Castillo, E. Rodríguez-González, M. Courel, Y. Sánchez, E. Saucedo, *J. Mater. Sci.: Mater. Electron.* **2018**, *29*, 15363.
[47] A. Fairbrother, M. Neuschitzer, E. Saucedo, A. Pérez-Rodríguez, *Phys. Status Solidi A* **2015**, *212*, 109.
[48] A. Fairbrother, M. Dimitrievska, Y. Sánchez, V. Izquierdo-Roca, A. Pérez-Rodríguez, E. Saucedo, *J. Mater. Chem. A* **2015**, *3*, 9451.
[49] A. Lafond, L. Choubrac, C. Guillot-Deudon, P. Deniard, S. Jobic, *Z. Anorg. Allg. Chem.* **2012**, *638*, 2571.
[50] G. Gurieva, R. Ferreira, P. Knoll, S. Schorr, *Phys. Status Solidi A* **2018**, *215*, 1700957.
[51] G. Gurieva, L. Elisa, V. Rios, A. Franz, P. Whitfield, S. Schorr, *J. Appl. Phys.* **2018**, *123*, 161519.
[52] L. E. Valle Rios, K. Neldner, G. Gurieva, S. Schorr, *J. Alloys Compd.* **2016**, *657*, 408.
[53] S. Chen, X. G. Gong, A. Walsh, S. H. Wei, *Phys. Rev. B: Condens. Matter Mater. Phys.* **2009**, *79*, 1.
[54] A. Hernandez Martinez, M. Placidi, L. Arques, S. Giraldo, Y. Sánchez, V. Izquierdo-Roca, P. Pistor, M. Valentini, C. Malerba, E. Saucedo, *ACS Appl. Energy Mater.* **2018**, *1*, 1981.
[55] S. Chen, J. H. Yang, X. G. Gong, A. Walsh, S. H. Wei, *Phys. Rev. B* **2010**, *81*, 245204.
[56] M. Dimitrievska, A. Fairbrother, E. Saucedo, A. Pérez-Rodríguez, V. Izquierdo-Roca, *Sol. Energy Mater. Sol. Cells* **2016**, *149*, 304.
[57] T. Nishimura, H. Sugiura, K. Nakada, A. Yamada, *Phys. Status Solidi RRL* **2018**, *12*, 1800129.
[58] A. Redinger, K. Hönes, X. Fontań, V. Izquierdo-Roca, E. Saucedo, N. Valle, A. Ṕrez-Rodríguez, S. Siebentritt, *Appl. Phys. Lett.* **2011**, *98*, 101907.
[59] S. Lopez-Marino, Y. Sánchez, M. Placidi, A. Fairbrother, M. Espindola-Rodríguez, X. Fontané, V. Izquierdo-Roca, J. Lopez-García, L. Calvo-Barrio, A. Pérez-Rodríguez, E. Saucedo, *Chem. - Eur. J.* **2013**, *19*, 14814.
[60] J. Just, D. Lützenkirchen-hecht, R. Frahm, S. Schorr, T. Unold, J. Just, D. Lu, *Appl. Phys. Lett.* **2011**, *99*, 262105.
[61] X. Fontané, L. Calvo-Barrio, V. Izquierdo-Roca, E. Saucedo, A. Pérez-Rodríguez, J. R. Morante, D. M. Berg, P. J. Dale, S. Siebentritt, *Appl. Phys. Lett.* **2011**, *98*, 181905.
[62] A. Fairbrother, V. Izquierdo-Roca, X. Fontané, M. Ibáñez, A. Cabot, E. Saucedo, A. Pérez-Rodríguez, *CrystEngComm* **2014**, *16*, 4120.
[63] A. Fairbrother, E. García-Hemme, V. Izquierdo-Roca, X. Fontané, F. A. Pulgarín-Agudelo, O. Vigil-Galán, A. Pérez-Rodríguez, E. Saucedo, *J. Am. Chem. Soc.* **2012**, *134*, 8018.
[64] C. J. Hages, S. Levcenco, C. K. Miskin, J. H. Alsmeier, D. Abou-Ras, R. G. Wilks, M. Bär, T. Unold, R. Agrawal, *Prog. Photovoltaics* **2015**, *23*, 376.
[65] S. Giraldo, M. Neuschitzer, T. Thersleff, S. Lopez-Marino, Y. Sánchez, H. Xie, M. Colina, M. Placidi, P. Pistor, V. Izquierdo-Roca, K. Leifer, A. Pérez-Rodríguez, E. Saucedo, *Adv. Energy Mater.* **2015**, *5*, 1501070.
[66] S. Kim, J. S. Park, A. Walsh, *ACS Energy Lett.* **2018**, *3*, 496.
[67] G. Rey, G. Larramona, S. Bourdais, C. Choné, B. Delatouche, A. Jacob, G. Dennler, S. Siebentritt, *Sol. Energy Mater. Sol. Cells* **2018**, *179*, 142.
[68] P. Schöppe, G. Gurieva, S. Giraldo, G. Martínez-Criado, C. Ronning, E. Saucedo, S. Schorr, C. S. Schnohr, *Appl. Phys. Lett.* **2017**, *110*, 043901.
[69] J. A. Aguiar, M. E. Erkan, D. S. Pruzan, A. Nagaoka, K. Yoshino, H. Moutinho, M. Al-Jassim, M. A. Scarpulla, *Phys. Status Solidi A* **2016**, *213*, 2392.
[70] A. D. Collord, H. Xin, H. W. Hillhouse, *IEEE J. Photovoltaics* **2015**, *5*, 288.
[71] C. J. Hages, N. J. Carter, R. Agrawal, T. Unold, *J. Appl. Phys.* **2014**, *115*, 234504.
[72] A. Redinger, D. M. Berg, P. J. Dale, S. Siebentritt, *J. Am. Chem. Soc.* **2011**, *133*, 3320.
[73] H. Xie, Y. Sánchez, S. López-Marino, M. Espíndola-Rodríguez, M. Neuschitzer, D. Sylla, A. Fairbrother, V. Izquierdo-Roca, A. Pérez-Rodríguez, E. Saucedo, *ACS Appl. Mater. Interfaces* **2014**, *6*, 12744.
[74] S. Giraldo, C. M. Ruiz, M. Espíndola-Rodríguez, Y. Sánchez, M. Placidi, D. Cozza, D. Barakel, L. Escoubas, A. Pérez-Rodríguez, E. Saucedo, *Sol. Energy Mater. Sol. Cells* **2016**, *151*, 44.
[75] K. Rawat, P. K. Shishodia, *Phys. Status Solidi RRL* **2016**, *10*, 890.
[76] Z. Tong, K. Zhang, K. Sun, C. Yan, F. Liu, L. Jiang, Y. Lai, X. Hao, J. Li, *Sol. Energy Mater. Sol. Cells* **2016**, *144*, 537.

[77] A. Carrete, A. Shavel, X. Fontane, J. Montserrat, J. Fan, M. Ibãnez, E. Saucedo, A. Peez-Rodríguez, A. Cabot, *J. Am. Chem. Soc.* **2013**, *135*, 15982.
[78] D. Tiwari, T. Koehler, X. Lin, R. Harniman, I. Griffiths, L. Wang, D. Cherns, R. Klenk, D. J. Fermin, *Chem. Mater.* **2016**, *28*, 4991.
[79] K. F. Tai, D. Fu, S. Y. Chiam, C. H. A. Huan, S. K. Batabyal, L. H. Wong, *ChemSusChem* **2015**, *8*, 3504.
[80] D. Tiwari, M. Cattelan, R. L. Harniman, A. Sarua, N. Fox, T. Koehler, R. Klenk, D. J. Fermin, *ACS Energy Lett.* **2018**, *3*, 2977.
[81] G. S. Gautam, T. P. Senftle, E. A. Carter, *Chem. Mater.* **2018**, *30*, 4543.
[82] S. Giraldo, M. Neuschitzer, M. Placidi, P. Pistor, A. Perez-Rodriguez, E. Saucedo, *IEEE J. Photovoltaics* **2016**, *6*, 754.
[83] S. Lee, K. J. Price, E. Saucedo, S. Giraldo, *Nanoscale* **2018**, *10*, 2990.
[84] S. Giraldo, T. Thersleff, G. Larramona, M. Neuschitzer, P. Pistor, K. Leifer, A. Perez-Rodriguez, C. Moisan, G. Dennler, E. Saucedo, *Prog. Photovoltaics* **2016**, *24*, 1359.
[85] M. Neuschitzer, J. Marquez, S. Giraldo, M. Dimitrievska, M. Placidi, I. Forbes, V. Izquierdo-Roca, A. Pérez-Rodriguez, E. Saucedo, *J. Phys. Chem. C* **2016**, *120*, 9661.
[86] J. Márquez, H. Stange, C. J. Hages, N. Schaefer, S. Levcenko, S. Giraldo, E. Saucedo, K. Schwarzburg, D. Abou-Ras, A. Redinger, M. Klaus, C. Genzel, T. Unold, R. Mainz, *Chem. Mater.* **2017**, *29*, 9399.
[87] M. Neuschitzer, M. Espindola-Rodriguez, M. Guc, J. Marquez, S. Giraldo, I. Forbes, A. Perez-Rodriguez, E. Saucedo, *J. Mater. Chem. A* **2018**, *6*, 11759.
[88] H. Xin, S. M. Vorpahl, A. D. Collord, I. L. Braly, A. R. Uhl, B. W. Krueger, D. S. Ginger, H. W. Hillhouse, *Phys. Chem. Chem. Phys.* **2015**, *17*, 23859.
[89] Z. Wang, N. Brodusch, R. Gauvin, G. P. Demopoulos, *Nano Energy* **2018**, *53*, 130.
[90] A. Mule, B. Vermang, M. Sylvester, G. Brammertz, S. Ranjbar, T. Schnabel, N. Gampa, M. Meuris, J. Poortmans, *Thin Solid Films* **2017**, *633*, 156.
[91] S. G. Haass, C. Andres, R. Figi, C. Schreiner, M. Bürki, Y. E. Romanyuk, A. N. Tiwari, *Adv. Energy Mater.* **2018**, *8*, 1701760.
[92] Y. Yang, L. Huang, D. Pan, *ACS Appl. Mater. Interfaces* **2017**, *9*, 23878.
[93] Y. Zhang, J. Han, C. Liao, *CrystEngComm* **2016**, *18*, 9026.
[94] Z. Y. Zhao, X. Zhao, *Inorg. Chem.* **2014**, *53*, 9235.
[95] H. Xie, S. López-Marino, T. Olar, Y. Sánchez, M. Neuschitzer, F. Oliva, S. Giraldo, V. Izquierdo-Roca, I. Lauermann, A. Pérez-Rodríguez, E. Saucedo, *ACS Appl. Mater. Interfaces* **2016**, *8*, 5017.
[96] S. Lopez-Marino, Y. Sanchez, M. Espindola-Rodriguez, X. Alcobe, H. Xie, M. Neuschitzer, I. Becerril, S. Giraldo, M. Dimitrievska, M. Placidi, L. Fourdrinier, V. Izquierdo-Roca, A. Perez-Rodriguez, E. Saucedo, *J. Mater. Chem. A* **2016**, *4*, 1895.
[97] I. Becerril-Romero, L. Acebo, F. Oliva, V. Izquierdo-Roca, S. López-Marino, M. Espíndola-Rodríguez, M. Neuschitzer, Y. Sánchez, M. Placidi, A. Pérez-Rodríguez, E. Saucedo, P. Pistor, *Prog. Photovoltaics* **2018**, *26*, 55.
[98] I. Becerril-Romero, S. Giraldo, S. López-Marino, M. Placidi, Y. Sánchez, D. Sylla, A. Pérez-Rodríguez, E. Saucedo, P. Pistor, *Sol. Energy Mater. Sol. Cells* **2016**, *154*, 11.
[99] K. S. Gour, O. P. Singh, A. K. Yadav, R. Parmar, V. N. Singh, *J. Alloys Compd.* **2017**, *718*, 231.
[100] T. Abzieher, T. Schnabel, M. Hetterich, M. Powalla, E. Ahlswede, *Phys. Status Solidi A* **2016**, *213*, 1039.
[101] S. G. Haass, C. Andres, R. Figi, C. Schreiner, M. Bürki, A. N. Tiwari, Y. E. Romanyuk, *AIP Adv.* **2018**, *8*, 015133.
[102] Z. Tong, C. Yan, Z. Su, F. Zeng, J. Yang, Y. Li, L. Jiang, Y. Lai, F. Liu, *Appl. Phys. Lett.* **2014**, *105*, 223903.
[103] S. Hartnauer, L. A. Wägele, E. Jarzembowski, R. Scheer, *Thin Solid Films* **2015**, *582*, 272.
[104] F. Jiang, Gunawan, T. Harada, Y. Kuang, T. Minegishi, K. Domen, S. Ikeda, *J. Am. Chem. Soc.* **2015**, *137*, 13691.
[105] D. A. R. Barkhouse, R. Haight, N. Sakai, H. Hiroi, H. Sugimoto, D. B. Mitzi, *Appl. Phys. Lett.* **2012**, *100*, 193904.
[106] B. Asenjo, C. Guilln, A. M. Chaparro, E. Saucedo, V. Bermudez, D. Lincot, J. Herrero, M. T. Gutirrez, *J. Phys. Chem. Solids* **2010**, *71*, 1629.
[107] C. Yan, F. Liu, K. Sun, N. Song, J. A. Stride, F. Zhou, X. Hao, M. Green, *Sol. Energy Mater. Sol. Cells* **2016**, *144*, 700.
[108] D. Cherns, I. J. Griffiths, L. Jones, D. M. Bishop, M. A. Lloyd, B. E. McCandless, *ACS Appl. Energy Mater.* **2018**, *1*, 6260.
[109] T. Thersleff, S. Giraldo, M. Neuschitzer, P. Pistor, E. Saucedo, K. Leifer, *Mater. Des.* **2017**, *122*, 102.
[110] Z. Yuan, S. Chen, Y. Xie, J. Park, H. Xiang, X. Gong, S. Wei, *Adv. Energy Mater.* **2016**, *6*, 1601191.
[111] G. Altamura, M. Wang, K. L. Choy, *Sci. Rep.* **2016**, *6*, 22109.
[112] Y.-T. Hsieh, Q. Han, C. Jiang, T.-B. Song, H. Chen, L. Meng, H. Zhou, Y. Yang, *Adv. Energy Mater.* **2016**, *6*, 1502386.
[113] S. Bag, O. Gunawan, T. Gokmen, Y. Zhu, T. K. Todorov, D. B. Mitzi, *Energy Environ. Sci.* **2012**, *5*, 7060.
[114] T. Taskesen, J. Neerken, J. Schoneberg, D. Pareek, V. Steininger, J. Parisi, L. Gütay, *Adv. Energy Mater.* **2018**, *8*, 1703295.
[115] S. Sahayaraj, G. Brammertz, B. Vermang, A. Mule, T. Schnabel, M. Meuris, J. Vleugels, J. Poortmans, *J. Mater. Chem. A* **2018**, *6*, 2653.
[116] G. Altamura, M. Wang, K.-L. Choy, *Sci. Rep.* **2016**, *6*, 22109.
[117] Y. S. Lee, T. Gershon, O. Gunawan, T. K. Todorov, T. Gokmen, Y. Virgus, S. Guha, *Adv. Energy Mater.* **2015**, *5*, 1401372.
[118] H. Tampo, K. M. Kim, S. Kim, H. Shibata, S. Niki, *J. Appl. Phys.* **2017**, *122*, 023106.
[119] K. Sun, F. Liu, J. Huang, C. Yan, N. Song, H. Sun, C. Xue, Y. Zhang, A. Pu, Y. Shen, J. A. Stride, M. Green, X. Hao, *Sol. Energy Mater. Sol. Cells* **2018**, *182*, 14.
[120] T. D. Lee, A. U. Ebong, *Renewable Sustainable Energy Rev.* **2017**, *70*, 1286.
[121] R. Kondrotas, F. Oliva, X. Alcobe, V. Izquierdo-Roca, A. Perez-Rodriguez, E. Saucedo, P. Pistor, *Prog. Photovoltaics* **2018**, *26*, 135.
[122] R. Caballero, C. Guillén, M. T. Gutiérrez, C. A. Kaufmann, *Prog. Photovoltaics* **2006**, *14*, 145.
[123] Z. K. Yuan, S. Chen, H. Xiang, X. G. Gong, A. Walsh, J. S. Park, I. Repins, S. H. Wei, *Adv. Funct. Mater.* **2015**, *25*, 6733.
[124] E. Chagarov, K. Sardashti, A. C. Kummel, Y. S. Lee, R. Haight, S. Talia, *J. Chem. Phys.* **2016**, *144*, 104704.
[125] T. Gershon, K. Sardashti, O. Gunawan, R. Mankad, S. Singh, Y. S. Lee, J. A. Ott, A. Kummel, R. Haight, *Adv. Energy Mater.* **2016**, *6*, 1601182.
[126] C. Ma, H. Guo, K. Zhang, N. Yuan, J. Ding, *Mater. Lett.* **2017**, *186*, 390.
[127] T. Gershon, Y. S. Lee, P. Antunez, R. Mankad, S. Singh, D. Bishop, O. Gunawan, M. Hopstaken, R. Haight, *Adv. Energy Mater.* **2016**, *6*, 1502468.
[128] J. Kumar, S. Ingole, *J. Alloys Compd.* **2017**, *727*, 1089.
[129] T. Gershon, K. Sardashti, Y. Seog, O. Gunawan, S. Singh, D. Bishop, A. C. Kummel, R. Haight, *Acta Mater.* **2017**, *126*, 383.
[130] Y. Zhao, X. Han, B. Xu, W. Li, J. Li, J. Li, M. Wang, C. Dong, P. Ju, J. Li, *IEEE J. Photovoltaics* **2017**, *7*, 874.
[131] J. Jia, Y. Li, B. Yao, Z. Ding, R. Deng, Y. Jiang, Y. Sui, *J. Appl. Phys.* **2017**, *121*, 215305.
[132] H. Guo, C. Ma, K. Zhang, X. Jia, Y. Li, N. Yuan, J. Ding, *Sol. Energy Mater. Sol. Cells* **2018**, *178*, 146.
[133] C. Ma, H. Guo, K. Zhang, Y. Li, N. Yuan, J. Ding, *Mater. Lett.* **2017**, *207*, 209.
[134] U. Saha, K. Alam, *RSC Adv.* **2018**, *8*, 4905.
[135] Y. Qi, Q. Tian, Y. Meng, D. Kou, Z. Zhou, W. Zhou, S. Wu, *ACS Appl. Mater. Interfaces* **2017**, *9*, 21243.

[136] Z. Xiao, Y. Li, B. Yao, R. Deng, Z. Ding, T. Wu, G. Yang, C. Li, L. Liu, L. Zhang, H. Zhao, *J. Appl. Phys.* **2013**, *114*, 183506.
[137] M. Pilvet, M. Altosaar, M. Grossberg, M. Danilson, K. Timmo, A. Mere, V. Mikli, *Thin Solid Films* **2015**, *582*, 180.
[138] Q. Zhang, H. Deng, L. Chen, L. Yu, J. Tao, L. Sun, P. Yang, J. Chu, *J. Alloys Compd.* **2017**, *695*, 482.
[139] L. Meng, B. Yao, Y. Li, Z. Ding, Z. Xiao, K. Liu, G. Wang, *J. Alloys Compd.* **2017**, *710*, 403.
[140] Z. Su, J. Ming, R. Tan, X. Li, X. Zeng, S. K. Batabyal, L. H. Wong, *Adv. Energy Mater.* **2015**, *4*, 2.
[141] C. Yan, K. Sun, J. Huang, S. Johnston, F. Liu, B. P. Veettil, K. Sun, A. Pu, F. Zhou, J. A. Stride, M. A. Green, H. Xiaojing, *ACS Energy Lett.* **2017**, *2*, 930.
[142] S. H. Hadke, S. Levcenko, S. Lie, C. J. Hages, J. A. Márquez, T. Unold, L. H. Wong, *Adv. Energy Mater.* **2018**, *8*, 1802540.
[143] S. Kim, K. M. Kim, H. Tampo, H. Shibata, K. Matsubara, S. Niki, *Sol. Energy Mater. Sol. Cells* **2016**, *144*, 488.
[144] A. D. Collord, H. W. Hillhouse, *Chem. Mater.* **2016**, *28*, 2067.
[145] S. Kim, K. M. Kim, H. Tampo, H. Shibata, S. Niki, *Appl. Phys. Express* **2016**, *9*, 1.
[146] R. Gunder, J. A. Márquez Prieto, G. Gurieva, T. Unold, S. Schorr, *CrystEngComm* **2018**, *20*, 1491.
[147] L. Choubrac, G. Brammertz, N. Barreau, L. Arzel, S. Harel, M. Meuris, B. Vermang, *Phys. Status Solidi A* **2018**, *215*, 1.
[148] S. Lie, M. Rui, W. Li, W. Leow, Y. F. Tay, D. M. Bishop, O. Gunawan, L. H. Wong, *J. Mater. Chem. A* **2018**, *6*, 1540.
[149] R. R. Prabhakar, S. Zhenghua, Z. Xin, T. Baikie, L. S. Woei, S. Shukla, S. K. Batabyal, O. Gunawan, L. H. Wong, *Sol. Energy Mater. Sol. Cells* **2016**, *157*, 867.
[150] R. Caballero, S. G. Haass, C. Andres, L. Arques, F. Oliva, V. Izquierdo-Roca, Y. E. Romanyuk, *Front. Chem.* **2018**, *6*, 1.
[151] S. Chatterjee, A. J. Pal, *Sol. Energy Mater. Sol. Cells* **2017**, *160*, 233.
[152] C. Yan, J. Huang, K. Sun, S. Johnston, Y. Zhang, H. Sun, A. Pu, M. He, F. Liu, K. Eder, L. Yang, J. M. Cairney, N. J. Ekins-Daukes, Z. Hameiri, J. A. Stride, S. Chen, M. A. Green, X. Hao, *Nat. Energy* **2018**, *3*, 764.
[153] M. Espindola-Rodriguez, D. Sylla, Y. Sánchez, F. Oliva, S. Grini, M. Neuschitzer, L. Vines, V. Izquierdo-Roca, E. Saucedo, M. Placidi, *ACS Sustainable Chem. Eng.* **2017**, *5*, 11516.
[154] P. D. Antunez, D. M. Bishop, Y. Luo, R. Haight, *Nat. Energy* **2017**, *2*, 884.
[155] T. P. White, N. N. Lal, K. R. Catchpole, *IEEE J. Photovoltaics* **2014**, *4*, 208.
[156] T. Shibuya, Y. Goto, Y. Kamihara, M. Matoba, K. Yasuoka, L. A. Burton, A. Walsh, *Appl. Phys. Lett.* **2014**, *104*, 021912.
[157] T. Kohl, G. Brammertz, J. de Wild, M. Neuwirth, M. Meuris, J. Poortmans, B. Vermang, *Thin Solid Films* **2018**, *660*, 247.
[158] T. Todorov, T. Gershon, O. Gunawan, C. Sturdevant, S. Guha, *Appl. Phys. Lett.* **2014**, *105*, 173902.
[159] C. Ros, T. Andreu, S. Giraldo, V. Izquierdo-Roca, E. Saucedo, J. R. Morante, *ACS Appl. Mater. Interfaces* **2018**, *10*, 13425.
[160] J.-J. Wang, J.-S. Hu, Y.-G. Guo, L.-J. Wan, *J. Mater. Chem.* **2011**, *21*, 17582.
[161] O. P. Singh, A. Sharma, K. S. Gour, S. Husale, V. N. Singh, *Sol. Energy Mater. Sol. Cells* **2016**, *157*, 28.
[162] K. S. Gour, O. P. Singh, B. Bhattacharyya, R. Parmar, S. Husale, T. D. Senguttuvan, V. N. Singh, *J. Alloys Compd.* **2017**, *694*, 119.
[163] K. S. Gour, B. Bhattacharyya, O. P. Singh, A. K. Yadav, S. Husale, V. N. Singh, *J. Alloys Compd.* **2018**, *735*, 285.
[164] H. Yang, L. A. Jauregui, G. Zhang, Y. P. Chen, Y. Wu, *Nano Lett.* **2012**, *12*, 540.
[165] X. Y. Shi, F. Q. Huang, M. L. Liu, L. D. Chen, *Appl. Phys. Lett.* **2009**, *94*, 122103.
[166] F.-J. Fan, B. Yu, Y.-X. Wang, Y.-L. Zhu, X.-J. Liu, S.-H. Yu, Z. Ren, *J. Am. Chem. Soc.* **2011**, *133*, 15910.
[167] F.-J. Fan, L. Wu, S.-H. Yu, *Energy Environ. Sci.* **2014**, *7*, 190.
[168] J. J. Scragg, T. Ericson, T. Kubart, M. Edoff, C. Platzer-Björkman, *Chem. Mater.* **2011**, *23*, 4625.
[169] B. Wang, H. Xiang, T. Nakayama, J. Zhou, B. Li, *Phys. Rev. B* **2017**, *95*, 035201.
[170] K. V. Gurav, S. W. Shin, U. M. Patil, P. R. Deshmukh, M. P. Suryawanshi, G. L. Agawane, S. M. Pawar, P. S. Patil, J. Y. Lee, C. D. Lokhande, J. H. Kim, *Sens. Actuators, B* **2014**, *190*, 408.
[171] N. M. Shinde, P. R. Deshmukh, S. V. Patil, C. D. Lokhande, *Sens. Actuators, A* **2013**, *193*, 79.